國 立 交 通 大 學

材料科學與工程學系

博 士 論 文

氧化鋯含量對莫來石/氧化鋯複合材料氧擴散與導電性之影響

Effect of Zirconia Content on Oxygen Diffusivities and Electrical Conductivities in Mullite/Zirconia Composites

研 究 生：柯宏達

指導教授：林健正 教授

中 華 民 國 九十八 年 九 月

氧化鋯含量對莫來石/氧化鋯複合材料氧擴散與導電性之影響

Effect of Zirconia Content on Oxygen Diffusivities and Electrical Conductivities in Mullite/Zirconia Composites

研 究 生：柯宏達　　Student：Hong-Da Ko

指導教授：林健正　　Advisor：Chien-Cheng Lin

國 立 交 通 大 學

材 料 科 學 與 工 程 學 系

博 士 論 文

A Thesis

Submitted to Department of Materials Science and Engineering

National Chiao Tung University

in partial Fulfillment of the Requirements

for the Degree of

Doctor of Philosophy

In

Materials Science and Engineering

September 2009

Hsinchu, Taiwan, Republic of China

中華民國九十八年九月

氧化鋯含量對莫來石/氧化鋯複合材料氧擴散與導電性之影響

研 究 生：柯宏達　　指導教授：林健正

國 立 交 通 大 學

材 料 科 學 與 工 程 學 系

摘 要

本研究利用三種不同方法測量莫來石/氧化鋯複合材料之氧擴散與電導。經由 ^{18}O-^{16}O 同位素交換反應並利用二次離子質譜儀(SIMS)可測得莫來石/氧化鋯複合材料的氧擴散係數；使用交流阻抗(AC impedance)量測莫來石/氧化鋯複合材料的電導；在氧分壓 20.2 到 2.02 kPa 範圍內，利用電導鬆弛法(conductivity relaxation method)可得到多孔莫來石/氧化鋯複合材料的氧擴散係數及表面交換係數。

同位素交換反應研究顯示，在溫度從 1000°C 到 1350°C 之間，氧化鋯含量 0 vol%～80 vol%之莫來石/氧化鋯複合材料其氧擴散係數為 10^{-21}～10^{-10} m^2/s。在氧化鋯含量 30 vol%與 40 vol%之間，氧擴散係數有著極大的變化。由於在高氧化鋯含量複合材料中氧化鋯相互連結形成一個快速路徑，而氧離子可經由此路徑移動。因此高氧化鋯含量複合材有較高的氧擴散係數。氧擴散之活化能隨著氧化鋯含量增加而有降低的趨勢。

在莫來石/氧化鋯複合材料的電導研究中，純氧化鋯與莫來石/氧化鋯複合材料的阻抗圖譜皆顯示兩個半圓，而此兩半圓分別是由材料中的晶粒及晶界所貢獻。純莫來石陶瓷的阻抗圖譜顯示一個半圓，而此半圓是由莫來石之晶粒所貢獻。莫來石/氧化鋯複合材料的電導隨著氧化鋯含量增加而增加。在交流頻率 1 MHz 測量下的導電度符合 Lichtenecker's rule 的預測，而在交流頻率 1 kHz 測量下的導電度則符合混合方程式(general mixing equation)。

在多孔莫來石/氧化鋯複合材料的研究中，高氧化鋯含量複合材料的表面交換係數趨近一常數。而低氧化鋯含量複合材的氧擴散與表面交換係數則隨著氧化鋯含量增加而增加。多孔莫來石/氧化鋯複合材料的表面交換係數存在一臨界體積分率在氧化鋯含量約 40 vol%左右。研究結果顯示低氧化鋯含量複合材的氧擴散係數與氧分壓無關，此是因為材料的氧擴散與其氧空孔息息相關，但氧空孔濃度不隨著氧分壓而變動。另外，高氧化鋯含量複合材料的表面交換係數則隨著氧分壓增加而減少。最後，經推測氧表面交換反應的速率決定步驟(rate-limiting step)應為電荷轉移過程(charge-transfer process)。

Effect of Zirconia Content on Oxygen Diffusivities and Electrical Conductivities in Mullite/Zirconia Composites

Hong-Da Ko, Ph. D.
Department of Materials Science and Engineering,
National Chiao Tung University, Hsinchu, Taiwan

Prof. Chien-Cheng Lin, Advisor

Abstract

Oxygen diffusivities and electrical conductivities in various mullite/PSZ composites were measured by $^{18}O/^{16}O$ isotope exchange method using secondary ion mass spectrometry and AC impedance spectroscopy, respectively. Additionally, oxygen diffusivities and surface exchange coefficients in various porous mullite/PSZ composites were measured at oxygen partial pressures ranging from 20.2 to 2.02 kPa using the conductivity relaxation method.

Oxygen diffusivities in mullite/PSZ composites exhibited a wide range of values from 10^{-21} to 10^{-10} m^2/s at temperatures between 1000 and 1350°C in the composites with 0 to 80 vol% PSZ. The percolation threshold occurred between 30 and 40 vol% PSZ, where oxygen diffusivities dramatically changed. There was a clear tendency of the activation energies of oxygen diffusion in composites to decrease with increasing PSZ contents. The large oxygen diffusivities in the high-PSZ composites were attributed to the interconnected channels of PSZ from the microstructural aspect.

For the measurement of electrical conductivities in mullite/PSZ composites, the impedance spectra of monolithic PSZ and mullite/PSZ composites showed two semicircles because of the contributions from grains and grain boundaries, while those of monolithic mullite had one semicircle due to the predominant contribution from grains. This indicates that the conductivities of the mullite/PSZ composites increased with PSZ content. While the conductivities of various composites at 1 MHz were fitted by Lichtenecker's rule, the general mixing equation could be applied to the conductivities measured at 1 kHz.

For the measurement of oxygen diffusivities and surface exchange coefficients in porous mullite/PSZ composites, oxygen diffusivities and surface exchange coefficients in low-PSZ composites increased with PSZ content, while the surface exchange coefficients in high-PSZ composites were approximately constant. A percolation threshold of the surface exchange coefficients took place at ~40 vol% PSZ for porous mullite/PSZ composites. The oxygen diffusivities in porous low-PSZ composites were independent of the oxygen partial pressure, implying that oxygen diffusion in these composites was related to the migration of oxygen vacancies, of which the concentration was independent of the oxygen partial pressure. The surface exchange coefficients of high-PSZ composites decreased with increasing oxygen partial pressure. Finally, it was found that the rate-limiting step for oxygen surface exchange could be the charge-transfer process.

誌 謝

博士研究生涯中，首先要感謝指導教授林健正老師，在實驗上給予許多教導與建議，讓學生了解研究該有的態度與想法，並令學生能完成博士學位。並由衷感謝所有口試委員們在論文的指正與建議。

感謝工研院材料研究所邱國創先生在研究材料電導性上的指導以及儀器上的協助。感謝所有畢業與在學的實驗室夥伴們，因為有了你們研究生活才會多采多姿。感謝璞玉計畫小組所有小姐們，你們的加油打氣，讓我備感窩心，也預祝璞玉計畫順利執行成功。

最後感謝我的家人與好友們，不管是生活或是精神上一直支持我，讓我的生活不虞匱乏。在大家的鼓勵與幫助下，終於完成了論文，在此獻給所有關心我及我所關心的朋友們！

Contents

List of Tables

List of Figures

Chapter 1
Introduction

1.1 Mullite and Zirconia

Mullite has become a potential material for advanced structural and functional ceramic because of its outstanding properties: low thermal expansion coefficient, good electrical insulation, high creep resistance, good high-temperature strength, and good chemical stability.[1, 2] There are wide applications for mullite and mullite-related composites in industry, since they are used as refractory materials, high-temperature engineering materials, electronic packaging materials, optical materials, etc.[1]

Mullite is the only stable crystalline phase in the SiO_2-Al_2O_3 binary system under atmospheric conditions. The lattice type of mullite is orthorhombic (space group *Pbam*) and lattice constants are a = 0.755 nm, b = 0.768 nm, c = 0.288 nm.[1] The chemical formula of mullite can be expressed as $Al_2[Al_{2+2x}Si_{2-2x}]O_{10-x}$, where x ($0.17 \leq x \leq 0.59$) is the number of missing oxygen atoms per unit cell. The formula represents the composition of sillimanite ($Al_2O_3 \cdot SiO_2$) for x = 0, while the formula shows the composition of stoichiometric mullite ($3Al_2O_3 \cdot 2SiO_2$) for x = 0.25.

Pure zirconia (ZrO_2) has three crystalline forms: monoclinic (T < 1200°C), tetragonal (1200°C < T < 2370°C) and cubic (T > 2370°C). The high temperature phases can be stabilized at room temperature by doped aliovalent oxides (e.g., Y_2O_3, MgO, CaO, etc.) to create fully stabilized zirconia (FSZ) or partially stabilized zirconia (PSZ).[3] The stabilizers not

only stabilize the cubic and tetragonal structures but also create oxygen vacancies as following equation:

$$Y_2O_3 \xrightarrow{ZrO_2} 2Y'_{Zr} + 3O^{\times}_{o} + V^{\circ\circ}_{O} \qquad (1.1)$$

A large number of oxygen vacancies will cause high oxygen-ion mobility in stabilized ZrO_2, because oxygen ionic conduction takes place by the movement of oxygen ions through oxygen vacancies. Therefore, ZrO_2 doped with aliovalent oxides has been attracted a great deal of attention for technological applications such as high temperature solid oxide fuel cells, oxygen sensors, and electrochemical oxygen pumps.[3, 4]

1.2 Mullite/Zirconia Composites

In order to enhance the mechanical properties of mullite ceramics, various mullite-matrix composites have been studied.[5-7] It is well known that the major toughening mechanism in ZrO_2-toughened mullite composite is the stress-induced phase transformation toughening.[8] Besides, the silicon carbide(SiC)-whisker is also the excellent reinforcement to improve the mechanical properties of mullite ceramics.[7, 9] However, the oxidation of SiC in mullite ceramics could cause the degradation of their mechanical properties under high-temperature oxidizing environments.

Two oxidation modes of SiC-reinforced mullite/ZrO_2 composites were described by Lin *et al*.[10] They proposed various oxidation modes based upon the relationship of the silica layer thickness and the depth of corresponding SiC whisker below the outermost surface in mullite/ZrO_2

composites at elevated temperatures. The oxidation behavior of ceramic-matrix composites closely depends upon the composition of the matrix in the composites. Tsai *et al.*[11, 12] reported that the oxidation behavior of SiC/ZrO_2/mullite composites depended upon the ZrO_2 content. When volume fraction of ZrO_2 in the matrix was smaller than a threshold value, the oxygen diffusivity was much slower in the matrix than in the SiO_2 layer and these composites morphologically showed a thinner oxidation zone. Conversely, the oxygen diffusivity was faster in the matrix than in the SiO_2 layer and these composites morphologically displayed a large oxidation zone when volume fraction of ZrO_2 was larger than the threshold value.

1.3 Thesis Outline

The oxidation behavior of SiC/ZrO_2/mullite composites correlates closely with the oxygen diffusion in the mullite/zirconia matrix. However, the investigation of oxygen diffusion in mullite/zirconia composites has not been presented to date. At first, the oxygen diffusivities in mullite/ZrO_2 composites were measured by $^{18}O/^{16}O$ isotope exchange method using secondary ion mass spectrometry (SIMS) and the effect of ZrO_2 content on oxygen diffusivities of mullite/ZrO_2 composites will be elucidated in Chapter 2.

The existence of oxygen vacancies in mullite and ZrO_2 can cause the oxygen ions to transport via oxygen vacancies. As a result, mullite and ZrO_2 can be applied as the solid electrolyte.[4, 13, 14] Because the physical properties of composite materials could be modified by a second phase, mullite/ZrO_2 composites should be considered as a potential solid electrolyte at elevated temperatures. The measurement of electrical properties in mullite/ZrO_2

composites is desirable. The electrical conductivities in mullite/ZrO_2 composites were measured by impedance spectroscopy and the influence of ZrO_2 content on electrical conductivity will be presented in Chapter 3.

For the reason that porous composites could be used in hot gas filtration environments, the influence of ZrO_2 content on diffusion and/or surface exchange rate in porous mullite/ZrO_2 composites is a notable subject. Few studies have been conducted on the character of mass transfer in porous mullite/ZrO_2 composites to date. The diffusivities and surface exchange coefficients of porous mullite/ZrO_2 composites with various ZrO_2 contents were measured by the conductivity relaxation method in this study. The effects of ZrO_2 content and oxygen partial pressure on the diffusivities and surface exchange coefficients of porous mullite/ZrO_2 composites will be explored in Chapter 4.

Chapter 5 will summarize the results obtained from Chapter 2 to Chapter 4.

Chapter 2

Oxygen diffusivities in mullite/zirconia composites measured by $^{18}O/^{16}O$ isotope exchange and secondary ion mass spectrometry

2.1 Introduction

Mullite-matrix composites are good candidates for high-temperature structural applications among ceramic-matrix composites, because of their low thermal expansion coefficient, excellent strength and creep resistance at high temperatures, and good thermal shock resistance. Previous studies have reported that PSZ and SiC effectively improved the mechanical properties of mullite-matrix composites.[5-7, 9] However, the oxidation of the SiC constituent would deteriorate the mechanical properties of such composites under high-temperature oxidizing environments. Moreover, the oxidation resistance of SiC-reinforced ceramic-matrix composites could be severely degraded because of the incorporation of PSZ into the matrix.

Several investigations on the oxidation behavior of mullite/PSZ/SiC composites have been carried out.[10-12, 15-17] In a pioneering study, Lin *et al*.[10] first phenomenologically proposed two distinct oxidation modes, designated as Mode I and Mode II, of mullite/PSZ/SiC composites at elevated temperatures: Mode I was based upon the assumption that oxygen diffusion in the silica layer was much faster than in the mullite/ZrO_2 matrix, and Mode II operated in opposite manner. However, oxygen diffusivities in various mullite/PSZ composites have not been available to date.

All the measurements of oxygen diffusivities in previous studies were conducted on monolithic ceramics.[18-20] Using SIMS, Fielitz *et al.*[18] measured oxygen diffusivities in 2/1-mullite and reported that oxygen diffusivities ranged from 5×10^{-20} to 9×10^{-18} m^2/s at temperatures ranging from 1250 to 1525ºC. Ikuma *et al.*[19] determined oxygen diffusivities in single crystal mullite to be between 1×10^{-21} and 8×10^{-20} m^2/s at 1100 to 1300ºC. Kim *et al.*[20] measured oxygen diffusivities in 2.8 mol% Y_2O_3-ZrO_2 as 3.5×10^{-11} m^2/s at 1000ºC using Raman spectroscopy combined with the ^{18}O-^{16}O isotope exchange technique. In this study, oxygen diffusivities in mullite/ZrO_2 composites with various ZrO_2 contents were measured by the $^{18}O/^{16}O$ isotope exchange method using SIMS, to supplement the existing data base of oxygen diffusivities in ceramic materials. The relationship among oxygen diffusivity, composition, and microstructure for various mullite/ZrO_2 composites is elucidated.

2.2 Experimental Procedures

The starting materials were commercial mullite powder (particle size = 0.2 μm in average, KM-mullite, Kyoritsu Ceramic Material Co., Nagoya, Japan) and 3 mol% Y_2O_3-doped PSZ powder (particle size = 0.3 μm in average, TZ-3Y, Toyo Soda Mfg., Co., Tokyo, Japan). The mullite powder was mixed with various amounts of PSZ. The compositions and designations of the composites are listed in Table 2.1.

The powder mixtures were hot pressed at 1600ºC, except at 1675ºC for the monolithic mullite, in an argon (Ar) atmosphere and a uniaxial pressure of 30 MPa for 45 min using a hot press (model HP50-HTG-7010, Thermal

Technology, Inc., Santa Rosa, CA). Oxygen-deficient PSZ was formed in the as-hot-pressed samples. To avoid the inaccuracy, the samples were preannealed in air at 1360ºC for 4 hours after ultrasonic cleaning in acetone so that stoichiometric ZrO_2 was obtained.

Hot-pressed samples were cut into pieces with dimensions of approximately 10 mm × 6 mm × 3 mm. All of the pieces were ground with a 15-μm diamond matted disc and then polished with 3-μm diamond paste using a precision polishing machine (model Minimet 1000, Buehler Ltd, Lake Bluff, IL). Then microstructures were observed by a field emission scanning electron microscope (FE-SEM, Model JSM-6500F, JEOL, Tokyo, Japan) with an acceleration voltage of 15 kV. To avoid charging, the samples were coated with gold using an ion coater.

The isotope-exchange method was applied using the rare stable isotope ^{18}O (99 at%, Isotec Inc., Miamisburg, OH, USA) as tracer. Prior to annealing, the samples were rinsed ultrasonically in an acetone bath and distilled water. Then the chamber was evacuated, and a mixture of Ar and ^{18}O with the ratio of 4:1 was introduced. The isotope exchange annealing was carried out at 1000°C/5 h, 1200°C/3 h, and 1350°C/2 h, respectively.

The isotope concentration profiles were analyzed using SIMS (Model Quad 6600, PHI, Chanhassen, MN, USA) with Cs ion (5 keV, 100 nA) as the primary beam. The rastered area was 300 μm × 300 μm, and the diameter of the analyzed zone was 75 μm. For the composites with a low-PSZ content (i.e., less than 30 vol% PSZ in this study), the diffusion depth of ^{18}O isotope was quite small, and the ^{18}O concentrations at various depths were

measured by sputtering with the Cs ion beam. In the case of the composites with a high-PSZ content (i.e., larger than 40 vol% PSZ in this study), the oxygen isotope penetrated deeply into the sample. The sample was then sectioned at various depths, where the ^{18}O concentrations were measured by the method mentioned previously.

2.3 Results and Discussion

2.3.1 Measured Oxygen Concentration Profiles

The concentrations of oxygen isotope were calculated from the measured secondary ion intensities $I(^{18}O)$ and $I(^{16}O)$ according to:

$$C(x,t) = \frac{I(^{18}O)}{I(^{16}O) + I(^{18}O)} \tag{2.1}$$

In general, it is better to determine diffusivities under conditions where the steady state is reached. To achieve such experimental conditions (large $\alpha(t/D)^{1/2}$), the measured ^{18}O concentration profiles can be fit by a simple erfc-type equation, while the reliability of the data can be improved by eliminating the surface exchange coefficient α as a fitting parameter. However, shorter diffusion anneal times (small $\alpha(t/D)^{1/2}$) were used in this study to expedite the experiments. Then oxygen diffusivities as well as surface exchange coefficients can be determined under such conditions, when the measured ^{18}O concentration profiles are fitted by the following diffusion solution $C(x,t)$ for a semi-infinite medium given by Crank.[21]

$$\frac{C(x,t)-C_{bg}}{C_g-C_{bg}} = \operatorname{erfc}\left(\frac{x}{\sqrt{4D_v t}}\right) - \exp\left(hx+h^2 D_v t\right)\operatorname{erfc}\left(\frac{x}{\sqrt{4D_v t}}+h\sqrt{D_v t}\right) \qquad (2.2)$$

where D_v is the volume diffusion coefficient (m^2/s), α the surface exchange coefficient (m/s), h being equal to α/D_v, C_g the ^{18}O concentration in the gas phase, C_{bg} the natural background level of ^{18}O in the sample (≈ 0.2%), and t the duration of the isotope anneal.

The ^{18}O concentration profiles $C(x,t)$ for various composites annealed at 1000°C are plotted in Fig. 2.1. The concentration profiles for MZY40 and MZY80 had a much smaller slope than those for pure mullite and for composites with 30 vol% PSZ or less. The slope of the concentration profile decreased with increasing PSZ content. As shown in Fig. 2.1(a), the tail for each composite approached a fixed value, which increased with PSZ content. This was probably caused by the fact that the grain boundary diffusion in PSZ is much higher than that in mullite. Note that the tail of experimental data in mullite was about 25 times higher than the natural ^{18}O content (0.2%) and about an order of magnitude higher than the grain-boundary-related tail of the diffusion profile as reported by Fielitz *et al.*[22] This could be attributed to the fact that the grain size (about 0.5 μm) in the current study was considerably smaller than that (about 5μm) in the previous study conducted by Fielitz *et al.*[22] The penetration depth of ^{18}O sharply increased as the PSZ content increased beyond some threshold value. Figure 2.1(b) shows the concentration profiles for MZY40 and MZY80, indicating a penetration depth of more than 70 μm. The ^{18}O concentrations of MZY80 were obviously higher than those of MZY40 at the corresponding depths.

2.3.2 Oxygen Diffusivities versus PSZ Contents

Oxygen diffusivities as well as surface exchange coefficients were determined from the ^{18}O concentration profiles $C(x,t)$, based upon Eqn. (2.2) and nonlinear regression analyses. The results are listed in Table 2.2. The composites were divided into two categories depending on their diffusivities and surface exchange coefficients: the composites with 30 vol% have smaller values for these parameters, and those with 40 vol% have larger values. Oxygen diffusivities in high-PSZ composites were thus about 8 orders of magnitude higher than those in low-PSZ composites. Furthermore, oxygen diffusivities in the low-PSZ composites ($\approx 10^{-21}$ to 10^{-18} m^2/s at 1000 to 1350°C) were close to that in pure mullite, while those in the high-PSZ composites ($\approx 10^{-11}$ to 10^{-10} m^2/s at 1000 to 1350°C) were close to that of zirconia.[20] It was also noted that oxygen diffusivity in mullite was unexpectedly larger than that in MZY05 or MZY15. This was attributed to the glassy phase typically at mullite grain triple junctions and grain boundaries because of the excess silica in mullite. It was believed that the oxygen transport through these grain boundaries, where the glassy phase was amorphous or liquidized at 1000 to 1350°C, was easier than through a crystalline phase.

Figure 2.2 illustrates the relationship of oxygen diffusivities with respect to PSZ content at different temperatures, indicating that there was a dramatic increase in oxygen diffusivities between 30 and 40 vol% PSZ at all the annealing temperatures. The dramatic change in oxygen diffusivities between MZY30 and MZY40 could be explained by the percolation theory[23, 24] and the effective medium theory.[25]

Bruggeman's symmetric effective medium theory assumes that two spherical particles are randomly mixed in the media. The diffusivity of such a random mixture (m), consisting of a high-diffusivity phase (h) and a low-diffusivity phase (l), can be predicted as follows: D_m = order of D_l, if $f < f_c$ and D_m = order of D_h, if $f > f_c$, where f is the volume fraction of the high-diffusivity phase and f_c is the percolation threshold. The percolation threshold f_c occurs at the volume fraction 0.33 for a three-dimensional case.

For the conductivity of a polymer-metal composite, the threshold decreased with increasing particle size ratio of the polymer with respect to the metal, as indicated in a previous study.[26] Carmona *et al*.[27] observed the threshold decreased with increasing aspect ratio of carbon fibers in the carbon-polymer composites.

In the present study, the high-diffusivity PSZ and the low-diffusivity mullite were equiaxed (or spherical) and both powders were randomly mixed. Therefore, the critical volume fraction between 30 and 40 vol% PSZ observed in this study is in agreement with the threshold value predicted by Bruggeman's symmetric effective medium theory.

Based on the measurements of SiO_2 layer (i.e., oxidation product of SiC) thickness at various depth beneath the outermost surface, Lin *et al*.[10] phenomenologically proposed two distinct oxidation modes of SiC/ZrO_2/mullite composites at elevated temperatures. Mode I shows a large gradient and a shallow oxidation depth, while Mode II exhibits a rather small gradient and a large oxidation depth.

Lin *et al.*[10] claimed that the oxidation behavior strongly depended on the relative oxygen diffusivities through the silica layer and the mullite/PSZ matrix as well, even though oxygen diffusivities in various matrices were not measured at all. In their proposal, Mode I was based on the assumption that oxygen diffusion in the silica layer was much faster than in the mullite/zirconia matrix, while Mode II was based on the opposite assumption.

The measured oxygen diffusivities in low-PSZ composites (≤ 30 vol% PSZ) were smaller by 3 to 4 orders of magnitude than that in SiO_2 (about 10^{-18} m^2/s at 1000ºC),[28] while those in high-PSZ composites (≥ 40 vol% PSZ) were higher by 5 to 6 orders of magnitude than that in SiO_2. These results could validate the modeling of oxidation modes proposed by Lin *et al.*[10]

It was worth noting that the ^{18}O concentration profiles in the present study resemble the SiO_2 layer thickness *versus* depth curves reported by Tsai and Lin.[12] Both experimental results (i.e., concentration profiles and SiO_2 layer thickness) of high-zirconia composites illustrated small gradients and large diffusion (or oxidation) depths, and *vice versa*. It was thus concluded that the oxidation behavior of SiC/ZrO_2/mullite composites is closely related to the oxygen diffusion through their respective ZrO_2/mullite matrices.

Fielitz and Borchardt[29] discussed the working limits of the diffusivities and surface exchange coefficients determined with the SIMS depth profile. They indicated that the chosen annealing time (t) with respect to the characteristic time constant (τ) was restricted to the range: $3\times10^{-4} \leq t/\tau \leq 10$ if the ^{18}O concentration at the surface reached about 80% of the gas

atmosphere and the dynamic range of the ^{18}O concentration was at least 1 order of magnitude higher than the natural abundance. The ratios of the experimental annealing time (t) to the characteristic time constant (τ) are listed in Table 2.2. It indicates that the t/τ ratios between 4.04×10^{-4} and 2.73×10^{-1} are in the limited range with sufficiently long annealing time so that the diffusivities and the surface exchange coefficients determined by Eqn. (2.2) have acceptable accuracies in the present study.

2.3.3 Activation Energies versus PSZ Contents

Figure 2.3 displays the Arrhenius plots of oxygen diffusivities *versus* $1/T$ for the composites with various PSZ contents. The activation energies of oxygen diffusion in the composites were determined by the slope of fitting lines and are listed in Table 2.3. The activation energy of oxygen diffusion in MZY40 was close to that in MZY80, while the activation energy of oxygen diffusion in MZY05 approached that in pure mullite. It was noted that the activation energy had a tendency to decrease with increasing PSZ content. However, the activation energy of oxygen diffusion in MZY30 was slightly larger than that in MZY20. The pre-exponential constant D_0 in the oxygen diffusivity expression $D= D_0\exp(-Q/RT)$ was determined from the intercept of the $\ln D$ *versus* $1/T$ plot and the results are listed in Table 2.3. It indicated much higher D_0 values for MZY40 and MZY80 than for others.

2.3.4 Microstructural Characteristics

The variation of oxygen diffusivities with respect to the PSZ content can be explained from the microstructural viewpoint. Figures 2.4(a) and 2.4(b) show the SEM micrographs of a low-PSZ and a high-PSZ composite, i.e., MZY15 and MZY40, respectively. The bright phase is PSZ, while the dark

one is mullite. Figure 2.4(a) reveals that the PSZ particles of MZY15 were isolated in the mullite matrix. In the low-PSZ composites, the oxygen diffused mainly via the continuous mullite, which has a small oxygen diffusivity (about 10^{-21} m^2/s at 1000ºC). This is why the oxygen diffusivities in low-PSZ composites were expected to be of the same order of the oxygen diffusivity in mullite. In contrast, Fig. 2.4(b) shows that the PSZ particles in MZY40 were interconnected. This interconnected channel of the PSZ phase, which had a high oxygen diffusivity of about 10^{-11} m^2/s at 1000ºC,[20] became a rapid diffusion path for oxygen in high-PSZ composites. It is thus expected that the oxygen diffusivities in high-PSZ composites are of the same order as the oxygen diffusivity in PSZ.

2.4 Conclusions

1. The oxygen diffusivities in various mullite/PSZ composites were measured by the $^{18}O/^{16}O$ isotope exchange and secondary ion mass spectrometry method. The oxygen diffusivities in mullite/PSZ composites ranged from 10^{-21} to 10^{-10} m^2/s, depending on the PSZ content and temperature.
2. The oxygen diffusivities in mullite/PSZ composites exhibited a threshold of PSZ content at between 30 and 40 vol%. The high-PSZ composites showed relatively high oxygen diffusivities, close to the oxygen diffusivity in PSZ. Correspondingly, the low-PSZ composites showed relatively small oxygen diffusivities, close to the oxygen diffusivity in mullite.
3. There was a clear tendency of the activation energies of oxygen diffusion in composites to decrease with increasing PSZ contents. The activation

energies of oxygen diffusion in high-PSZ composites were close to that of PSZ; while those of low-PSZ composites approached that of mullite.

4. The extreme difference in oxygen diffusivities between low-PSZ and high-PSZ composites was explained by the microstructural features of the composites. In the high-PSZ composites, the relatively large oxygen diffusivities were attributed to the interconnected PSZ channels, which provided a fast diffusion path for oxygen.

Table 2.1 Designations, compositions, hot-pressing conditions, and relative densities of various mullite/PSZ composites

Sample	Composition	HP Condition*	Relative Density (%)
M	mullite	1675ºC/45min	97.8
MZY05	95 vol.% mullite + 5 vol.% 3Y-PSZ	1600ºC/45min	97.1
MZY15	85 vol.% mullite + 15 vol.% 3Y-PSZ	1600ºC/45min	95.1
MZY20	80 vol.% mullite + 20 vol.% 3Y-PSZ	1600ºC/45min	95.4
MZY30	70 vol.% mullite + 30 vol.% 3Y-PSZ	1600ºC/45min	96.7
MZY40	60 vol.% mullite + 40 vol.% 3Y-PSZ	1600ºC/45min	97.5
MZY80	20 vol.% mullite + 80 vol.% 3Y-PSZ	1600ºC/45min	97.7

*All under the pressure of 30MPa and 1 atm argon

Table 2.2 Measured oxygen diffusivities (D), surface exchange coefficients (α), and characteristic time constants (τ) in various composites

Sample	Temp.(°C)	Time(sec)	D(m^2/s)	α(m/s)	τ (s)*	t/τ
M	1000	18000	3.3×10^{-21}	2.2×10^{-13}	6.60×10^{4}	2.73×10^{-1}
MZY05	1000	18000	1.7×10^{-21}	1.3×10^{-13}	1.03×10^{5}	1.76×10^{-1}
MZY15	1000	18000	3.6×10^{-21}	1.3×10^{-13}	2.04×10^{5}	8.81×10^{-2}
MZY20	1000	18000	1.6×10^{-20}	3.6×10^{-13}	1.25×10^{5}	1.44×10^{-1}
MZY30	1000	18000	2.2×10^{-20}	2.4×10^{-13}	3.93×10^{5}	4.57×10^{-2}
MZY40	1000	18000	1.4×10^{-12}	1.3×10^{-9}	9.13×10^{5}	1.97×10^{-2}
MZY80	1000	18000	3.8×10^{-12}	2.9×10^{-9}	4.46×10^{5}	4.04×10^{-2}
M	1200	10800	4.8×10^{-20}	2.5×10^{-13}	7.85×10^{5}	1.38×10^{-2}
MZY05	1200	10800	2.2×10^{-20}	1.1×10^{-13}	1.93×10^{6}	5.60×10^{-3}
MZY15	1200	10800	3.3×10^{-20}	1.6×10^{-13}	1.31×10^{6}	8.24×10^{-3}
MZY20	1200	10800	1.1×10^{-19}	2.6×10^{-13}	1.56×10^{6}	6.92×10^{-3}
MZY30	1200	10800	1.3×10^{-19}	2.0×10^{-13}	3.10×10^{6}	3.48×10^{-3}
MZY40	1200	10800	2.1×10^{-11}	1.2×10^{-9}	1.34×10^{7}	8.06×10^{-4}
MZY80	1200	10800	3.4×10^{-11}	2.0×10^{-9}	8.23×10^{6}	1.31×10^{-3}
M	1350	7200	1.1×10^{-18}	7.1×10^{-13}	2.21×10^{6}	3.25×10^{-3}
MZY05	1350	7200	5.6×10^{-19}	4.8×10^{-13}	2.44×10^{6}	2.95×10^{-3}
MZY15	1350	7200	6.4×10^{-19}	5.8×10^{-13}	1.90×10^{6}	3.79×10^{-3}
MZY20	1350	7200	1.4×10^{-18}	6.8×10^{-13}	3.09×10^{6}	2.33×10^{-3}
MZY30	1350	7200	2.6×10^{-18}	8.4×10^{-13}	3.68×10^{6}	1.96×10^{-3}
MZY40	1350	7200	6.4×10^{-11}	2.6×10^{-9}	9.75×10^{6}	7.38×10^{-4}
MZY80	1350	7200	1.9×10^{-10}	3.2×10^{-9}	1.78×10^{7}	4.04×10^{-4}

* $\tau = D/\alpha^2$

Table 2.3 Pre-exponential constants (D_0) and activation energies (Q) in various composites

	D_0 (m^2/s)*	Q (kJ/mol)
M	$6.7\ (\pm 0.50)\times 10^{-10}$	277 (±24)
MZY05	$2.9\ (\pm 0.26)\times 10^{-10}$	277 (±29)
MZY15	$3.5\ (\pm 0.38)\times 10^{-11}$	246 (±33)
MZY20	$6.4\ (\pm 0.79)\times 10^{-12}$	212 (±30)
MZY30	$2.4\ (\pm 0.36)\times 10^{-11}$	223 (±48)
MZY40	$8.1\ (\pm 0.38)\times 10^{-5}$	188 (±15)
MZY80	$2.0\ (\pm 0.10)\times 10^{-4}$	189 (±14)

*$D = D_0 \exp(-Q/RT)$

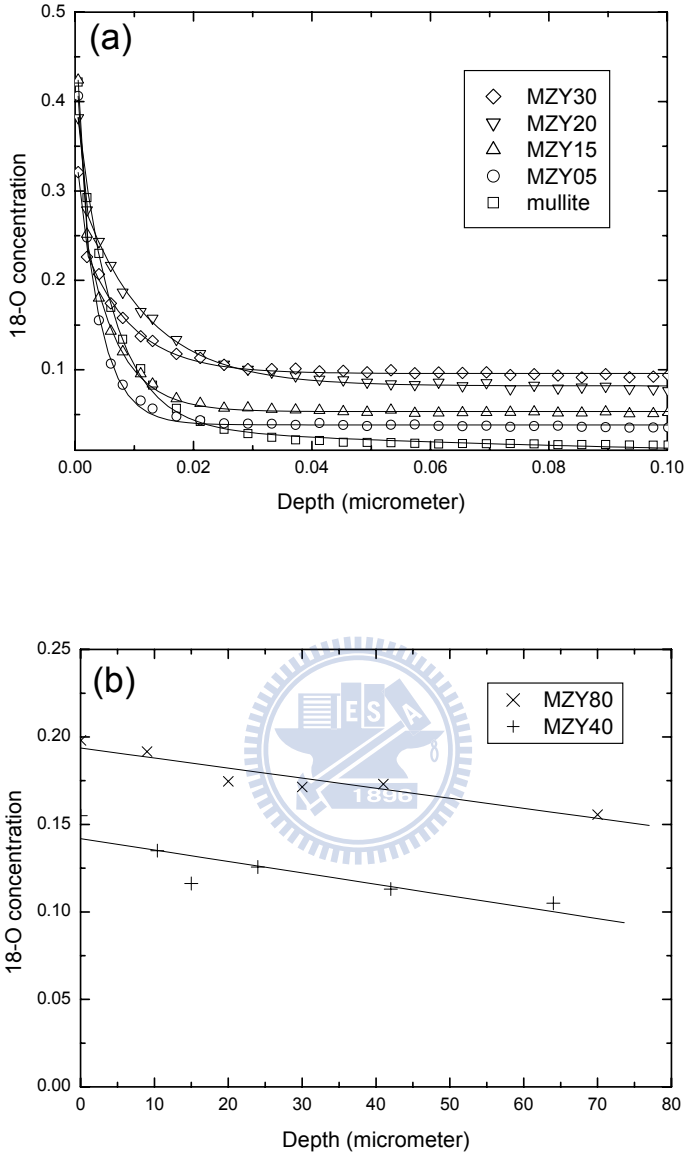

Fig. 2.1 The concentration profiles of oxygen isotope ^{18}O after annealing at 1000°C/5 h for (a) mullite, MZY05, MZY15, MZY20, and MZY30; (b) MZY40 and MZY80.

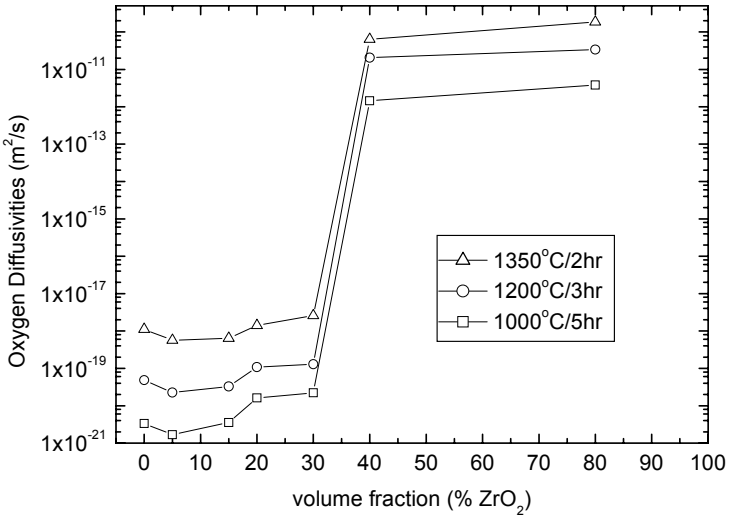

Fig. 2.2 The relationships of oxygen diffusivity and PSZ content after annealing at 1350°C/2 h, 1200°C/3 h and 1000°C/5 h, respectively.

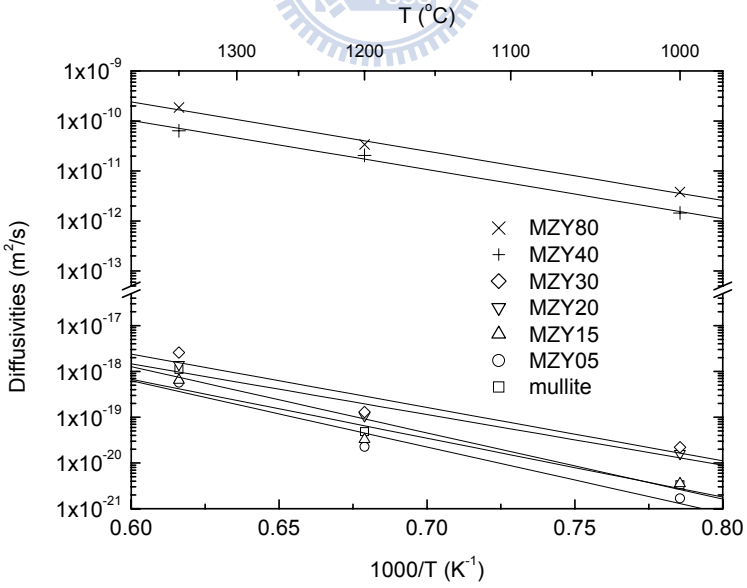

Fig. 2.3 Arrhenius plots of oxygen diffusivities in the composites with various PSZ contents.

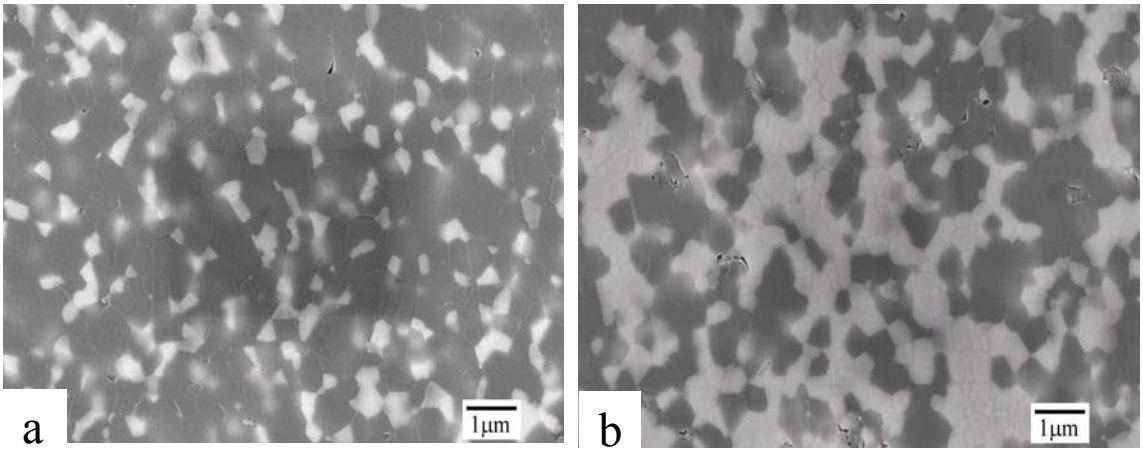

Fig. 2.4 Secondary electron images of the as hot-pressed (a) MZY15 and (b) MZY40. The bright phase is PSZ, while the dark phase is mullite. (Thermal etching at 1300ºC/1 h).

Chapter 3

Effect of zirconia content on electrical conductivities of mullite/zirconia composites measured by impedance spectroscopy

3.1 Introduction

Although mullite has good high temperature strength and chemical stability, its low toughness limits its use in advanced structural applications. The mechanical properties of PSZ/mullite, SiCw/mullite, and SiCw/PSZ/mullite composites have been studied by many investigators.[9, 30-33] It is well known that partially-stabilized zirconia (PSZ) and/or SiC whiskers can significantly improve the mechanical properties of mullite via mechanisms such as phase transformation toughening, whisker bridging, and crack deflection.

As far as electrical properties are concerned, mullite is a good insulator at room temperature and can be considered a semiconductor at high temperatures.[34, 35] Gerhardt and Ruh[36] reported that the incorporation of SiC-whiskers significantly affected the electrical properties of mullite matrix composites because SiC has a large dielectric constant (42 for SiC and 6.5 for mullite at 1 MHz)[37] and a small electrical resistivity (5×10^{5} ohm-cm for SiC and 1×10^{13} ohm-cm for mullite at room temperature)[38, 39] with respect to mullite. Previous studies have also been conducted on other composites.[40, 41] Gerhardt[40] showed the influence of volume fraction, size, and shape of reinforcing agents on the electrical properties of ceramic matrix and polymer

matrix composites. Runyan *et al.*[41] studied the electrical conductivities of BN-B_4C and BN-SiC composites under different orientations of the applied electrical field, and the results were fit by the McLachlan equation or general effective medium equation. It is believed that the dramatic change in electrical properties with respect to the volume fraction is attributable to the formation of interconnected channels of the good conducting phase within the composites.

For electrochemical applications, mullite and ZrO_2 can be used as the solid electrolyte of an oxygen concentration cell because oxygen ions can transport through oxygen vacancies.[4, 13, 14] Since the physical and/or chemical properties of composite materials could be tailored by incorporating various amounts of a second phase into a suitable matrix, a mullite/ZrO_2 composite should be considered as a potential solid electrolyte at elevated temperatures as well. The properties of composites, however, could be dependent on the intrinsic nature and the volume fractions of their constituents. Because there is a lack of literature on the subject, it is desirable to have a measurement of the electrical properties of mullite/zirconia composites. Therefore, the effect of ZrO_2 content on the electric conductivities is elucidated in this study.

3.2 Experimental Procedures

The raw materials used in this study were commercial mullite powder (with a nominal composition 71.86 wt% Al_2O_3, 28.07 wt% SiO_2, 0.03 wt% Fe_2O_3, 0.03 wt% NaO_2 and 0.01 wt% MgO_2, KM-mullite, Kyoritsu Ceramic Materials Co., Nagoya, Japan) and 3 mol% Y_2O_3 PSZ powder (3Y-PSZ, with

a nominal composition 94.75 wt% ZrO_2, 5.21 wt% Y_2O_3, 0.005 wt% Al_2O_3, 0.005 wt% SiO_2, 0.002 wt% Fe_2O_3 and 0.022 wt% NaO_2, TZ-3Y, Toyo Soda Mfg., Co., Tokyo, Japan).

The PSZ content in the mullite/PSZ composites was in the range from 5 to 80 vol%. The sample containing 5 vol% 3Y-PSZ was designated MZY05. Others were designated in a similar way with "M" and "Z" standing for monolithic mullite and 3Y-PSZ, respectively. The designations, compositions, hot pressing conditions, and relative densities of various composites are listed in Table 3.1.

Experimental samples were fabricated by hot-pressing at a temperature of 1675ºC for pure mullite and at 1600ºC for mullite/PSZ composites in argon at a pressure of 30 MPa for 45 min (Model HP50-HTG-7010, Thermal Technology Inc., Santa Rosa, CA). After hot pressing, the PSZ in the composites became oxygen deficient and blackened. The hot-pressed composites and PSZ were then annealed at 1360ºC/4 h in air so that near stoichiometric PSZ was obtained. Bulk densities were measured by the Archimedes method using deionized water as an immersion medium. The phases in each composite were identified using an x-ray diffractometer (XRD, Model MXP18, Mac Science, Yokohama, Japan). The measuring conditions of the XRD were Cu K_α radiation at 50 kV, 150 mA and a scanning rate of 2°/min. The PSZ contained both monoclinic and tetragonal phases in all composites as shown in Table 3.1.

Microstructures were characterized by SEM (Model JSM-6500, JEOL, Tokyo, Japan). The SEM specimens were cut into pieces about 5 × 6 × 0.5

mm, ground, and polished with diamond paste using standard procedures.

The Pt paste diluted with alcohol was painted on the surface of each sample and fired at 1000°C/10 min to prepare the electrode. Then, the sample was placed on a Pt plate. Two Pt wires were used to connect the sample to the measuring system, one contacted to the Pt electrode and the other to the Pt plate. The conductivity measurements were carried out by an alternating current (ac) impedance spectroscope (Model 4194A, Hewlett Packard Co., Palo Alto, CA. USA) in the frequency range of 100 Hz to 10 MHz at temperatures between 150 and 1300°C in air. The impedance-measuring system is schematically shown in Fig. 3.1. The impedance data were analyzed and fitted using the electrochemical impedance software, Z-view.[42]

3.3 Results and Discussion

3.3.1 Analyses of Impedance Spectra

The impedances of mullite and low-PSZ composites were found to be extremely large and scattered with significant errors at T≤ 300ºC. Their impedances were large enough so that the effect of inductive reactance was negligible. In the other respect, the impedance data of PSZ and high-PSZ composites at high temperatures were not adopted due to the inductive reactance. The Pt electrodes painted on the samples were porous and therefore could be regarded as several small metal wires. The electric current through the porous Pt electrode induced the inductive reactance, which adversely affected the conductivity measurements of PSZ and high-PSZ composites. Some of the measured impedance data in the high-frequency impedance spectra of PSZ and high-PSZ composites has a

positive reactance. These data were unable to be analyzed and it was noted that the degree of deviation from negative values increased with temperature. At high temperatures, PSZ behaves like a fast ion conductor, and the effect of inductive reactance becomes more apparent. Thus, one could not accurately obtain their electrical properties from the data measured at high frequencies and high temperatures.

Figure 3.2(a) shows the typical impedance spectra for MZY10 at temperatures ranging from 400 to 1000^{o}C. The horizontal axis is the real part of impedance (or resistance) while the vertical axis is the corresponding imaginary part (or reactance). The frequencies increased from right to left along the horizontal axis. The shape of the impedance spectra for MZY10 did not change significantly with respect to temperature, but the overall values of impedance did sharply decrease with temperature. Figure 3.2(b) shows the impedance spectra for MZY80 at temperatures between 200 and 450^{o}C, with two distinct semicircles in each impedance spectrum. The two semicircles corresponding to high and low frequencies in the impedance spectra of MZY80 were related to grains and grain boundaries, respectively.[43, 44] The resistivities of MZY10 and MZY80 decreased with increasing temperature in the same way exhibited by the general ceramics. This is caused by the so-called negative temperature coefficient (NTC) behavior.

Figure 3.3 shows the impedance spectra of the composites with various PSZ contents at fixed temperatures. Note that the resistivities decrease with increasing PSZ content because PSZ, which is known to be a good ionic conductor, has a much smaller resistivity than mullite. Figure 3.3(a) shows

only one semicircle in the impedance spectrum of monolithic mullite at 700ºC. Monolithic mullite shows similar behavior, as reported in pervious studies.[45, 46] The relaxation frequencies for mullite were estimated to be between 20 kHz and 1 MHz at temperatures ranging from 500 to 1300°C. The semicircle in the impedance spectra of mullite could be caused by the predominant contribution of grains because of the high relaxation frequency values.[46]

Meng and Huggins[47] indicated that oxygen ionic conduction could be expected in mullite when oxygen vacancies were created by the substitution of Al^{3+} for Si^{4+} in the sillimanite structure. Hirata *et al*.[48] reported that the electrons in mullite could be excited to the conduction band at a low oxygen pressure and that the electrical conduction of mullite is a combination of electronic and ionic conduction in a nitrogen atmosphere. In this study, the electrical conduction in mullite should be ionic conduction since the measurements were conducted in air.

The impedance spectra of monolithic PSZ and MZY80, as shown in Fig. 3.3(b), clearly revealed two semicircles that were related to grains and grain boundaries of PSZ. The impedance spectra of mullite/PSZ composites other than MZY80, however, were unlike those of monolithic mullite and PSZ, as shown in Figs. 3.3(a) and 3.3(b). The impedance responses at high and low frequencies showed two partially overlapped semicircles. Note that the low- and high-frequency arcs in impedance spectra were gradually discernible as the PSZ content was increased.

3.3.2 Conductivities and Activation Energies

The impedance data of PSZ and PSZ/mullite composites can be divided into two semicircles corresponding to high and low frequencies. They were modeled by an equivalent circuit consisting of two R-CPE parallel circuits in series, where R and CPE are the resistor and the constant-phase element, respectively.[49] The impedance spectra of monolithic mullite showed , however, a single imperfect semicircle (i.e., a depressed circular arc), and its data were fit using a model of one R-CPE parallel circuit.[49] In the other way, the impedance spectra with a perfect semicircle would be fit by the equivalent circuit of one RC parallel circuit.

The conductivities of various composites obey the Arrhenius equation and can be expressed by:

$$\sigma T = A \exp\left(-\frac{E_a}{RT}\right) \tag{3.1}$$

where σ is the conductivity (ohm^{-1} cm^{-1}), A is a constant, E_a is the activation energy (kJ/mol), R is the gas constant (J/mol K), and T is the absolute temperature (K).

Figure 3.4 displays the Arrhenius plots of ln(σT) as a function of 1/T for all samples. The conductivities of the composites in the high-frequency region increased with increasing PSZ content as shown in Fig. 3.4(a). In contrast, the plots in Fig. 3.4(b) indicate that the conductivities in the low-frequency region exhibited a somewhat different trend. The conductivities of MZY20 at low temperatures were smaller than those of MZY05 and MZY10.

Furthermore, the slope of the ln(σT) *versus* 1/T curve for MZY20 was much larger than those for MZY05 and MZY10. The electrical conductivity versus 1/T curves of MZY30, MZY40, or MZY50 demonstrate a similar slope.

It was also noted that the conductivity in the high-frequency region (related to grains) of MZY80 was the same as that of PSZ, while the conductivity in the low-frequency region (related to grain boundaries) was much lower than that of PSZ. This can be explained by the fact that mullite grains are located at the grain boundaries of PSZ and the existence of intergranular mullite slightly decreased the conductivity of MZY80 along the grain boundaries. The intergranular mullite, however, did not affect the conductivity across the dense interconnected channels of PSZ grains in MZY80.

Figure 3.5 displays the activation energies of electrical conduction with respect to PSZ content in the high- and low-frequency regions. The activation energy for mullite was found to be about 65 kJ/mol, which is in agreement with previous studies.[45, 47] For PSZ, the activation energies of the grain conductivity at high frequencies and of the grain-boundary conductivity at low frequencies were found to be about 79 and 93 kJ/mol, respectively, agreeing with the results reported by Guo and Zhang.[44]

The activation energies in the high- and low-frequency regions for MZY05 and MZY10 are approximately the same as that for mullite. The high-frequency measurements of MZY05 and MZY10 could be correlated with the presence of grains of mullite. The grain conductivities of MZY05

and MZY10, however, were different from those of monolithic mullite. PSZ has a much lower resistivity than mullite and can affect the electrical response in MZY05 and MZY10. That is why the grain conductivities for MZY05 and MZY10 are so different with those for monolithic mullite.

In contrast, the low-frequency regions for MZY05 and MZY10 were correlated to the grain boundaries of PSZ and/or mullite. While a glassy phase was usually observed in the grain boundaries of monolithic mullite, the composites containing PSZ were lacking a glassy phase.[50, 51] For MZY05 and MZY10, the low-frequency signal would transport through grain boundaries of mullite and/or PSZ instead of the glassy phase.

When the PSZ content was larger than 20 vol%, the activation energies in the low-frequency region were much higher than those of MZY05 and MZY10. This could be explained by the formation of a space charge layer at the interface of mullite and PSZ grains in an electric field. The space charge layer is usually formed at the interface of two phases with dissimilar electrical properties. The presence of a space charge potential would increase the activation energy of the electric conduction through the grain boundaries.[44] Therefore, the low-frequency arcs of the composites were related to the space charge contribution when the PSZ content was larger than 20 vol%. There was not much difference in the activation energies from MZY20 to MZY60 at low frequencies. In contrast, the activation energies of the electric conduction in the high-frequency region between MZY20 and MZY60 increased gradually with PSZ content.

Figure 3.5 also shows that the activation energies of the electric conduction

for MZY80 were close to those values for PSZ in the corresponding high- and low-frequency regions.

3.3.3 Conductivity versus PSZntent

Various theories describe the physical properties of a multi-phase system. The general mixing equation is frequently used to predict the electrical properties of a heterogeneous system and can be expressed by:[52]

$$\sigma_c^{\,n} = (1-V)\sigma_m^{\,n} + V\sigma_z^{\,n} \tag{3.2}$$

where V is the volume fraction of PSZ, σ_m, σ_z and σ_c are the conductivities of mullite, PSZ, and composite, respectively, and n is a constant between -1 and 1. For the extreme, case, $n = 1$ if these two phases are laminated and laid parallel to the direction of electric current; $n = -1$ if these two phases are laminated and laid perpendicular to the direction of electric current. There is a mixed case where $-1 < n < 1$. When $n \rightarrow 0$, the mixing equation is given by:[52]

$$\log\sigma_c = (1-V)\log\sigma_m + V\log\sigma_z \quad . \tag{3.3}$$

This expression was first proposed by Lichtenecker and was called Lichtenecker's rule.[53] The empirical Lichtenecker's rule was applied successfully to estimate the dielectric content of a two-phase system in previous studies.[54, 55] Zakri *et al*.[56] demonstrated that Lichtenecker's rule is not only an empirical relationship based on experimental results, but also a theoretical model that can be derived from the effective medium theory.

To understand the change of electrical properties in composites with various PSZ contents, the resistance (R) of those samples was measured at some fixed low and high frequencies. Then, the conductivity (σ) was calculated using:

$$\sigma = \frac{1}{R} \cdot \frac{l}{A} \tag{3.4}$$

where l and A were the thickness and cross-sectional area of the sample perpendicular to the electric current direction, respectively.

Figures 3.6(a) and 3.6(b) display the real parts of conductivity (σ') as a function of PSZ content at the frequencies of 1 kHz and 1 MHz, respectively, at 600^{o}C, indicating that the real part of conductivity increases with PSZ content. It was noted that the plot of ln σ' *versus* PSZ content at 1 MHz [Fig. 3.6(a)] demonstrates a linear behavior in agreement with Lichtenecker's rule. Figure 3.6(b), however, shows that the conductivities measured at 1 kHz with various PSZ contents were fit using the mixing rule [Eqn. (3.2)]. The parameter n was about 0.25.

The different trends for the ln σ' of composites with various PSZ contents at 1 MHz and 1 kHz were caused by different factors. The conductivities measured at 1 MHz and 1 kHz were gained from the contribution of grains and grain boundaries, respectively. Figure 3.6(b) shows that the conductivities of composites with 30 to 60 vol% PSZ were not much different from the conductivities measured at 1 kHz. This could result from

the existence of space charge at grain boundaries as mentioned previously. Thought the space charge layer could deplete the charge carriers and cause an increase in resistivity of the grain boundaries,[44] the resistivity was expected to decrease with increasing PSZ content. These two conflicting factors on the resistivity of grain boundaries resulted in less difference in the conductivity at 1 kHz when the PSZ content was between 30 and 60 vol%.

Oxygen diffusivities of mullite/PSZ composites with various PSZ contents show percolation behavior with respect to PSZ content,[57] though percolation behavior of electrical conductivities was not observed for mullite/PSZ composites. This could be attributed to less difference in the conductivities between mullite and PSZ. The oxygen diffusivity of PSZ was larger than that of mullite by at least 8 orders of magnitude; however, the difference in electrical conductivities at 1 MHz between mullite and PSZ was only about 2 orders of magnitude. Hence, the electrical conductivities of the composites do not reveal the percolation behavior.

3.3.4 Microstructural View of Point

Figure 3.7 shows that MZY05 exhibited elongated grains of mullite, while mullite grains in MZY30 and MZY80 were equiaxed. From the SEM micrograph of MZY05 [Fig. 3.7(a)], it was concluded that PSZ was located at the grain boundaries of mullite and was isolated by mullite grains. It was inferred that the conductivity was still dominated by mullite as mentioned in previous section, although the grain conductivity in MZY05 was increased because of the addition of PSZ. Figure 3.7(b) reveals that some PSZ particles became interconnected in MZY30. The conductivity would be

significantly affected by PSZ. Figure 3.7(c) showed that mullite grains were surrounded by PSZ grains in MZY80. The rapid path of interconnected PSZ for electrical conductivity was formed in MZY80, and the grain and grain-boundary conductivities in MZY80 were completely controlled by PSZ.

3.4 Conclusions

1. The electrical conductivities of mullite/PSZ composites with PSZ content were measured by the ac impedance spectroscopy. The impedance spectra of monolithic mullite showed only one semicircle, while the monolithic PSZ and mullite/PSZ composites showed two semicircles.
2. The conductivities of mullite/PSZ composites increased with the PSZ content, but no percolation relationship was observed. The real parts of conductivities measured at 1 MHz and 1 KHz were in good agreement with the Lichtenecker's rule and the mixing rule, respectively.
3. The activation energies of electrical conduction for mullite/PSZ composites were different in the high-frequency and low-frequency regions, depending on the PSZ content. The activation energies of grain conductivities in mullite and PSZ were about 65 and 79 kJ/mol, respectively, while those in the composites were calculated in between these two values. Furthermore, the activation energies sharply increased at 10 to 20 vol% PSZ in the low-frequency region.
4. The electrical conductivities of mullite/PSZ composites were effectively increased by the incorporation of PSZ so that high-PSZ composites

could be used for electrochemical purposes such as a gas sensor at high temperatures.

Table 3.1 Designations, compositions, hot pressing conditions, relative densities, and x-ray phases of various mullite/PSZ composites

Designation	Composition*	Hot Pressing Condition[#]	Relative Density (%)	XRD Phases*
M	100 v/o M	1675°C/45 min	97.8	M
MZY05	95 v/o M + 5 v/o Z	1600°C/45 min	97.1	M, *t*-Z, *m*-Z
MZY10	90 v/o M + 10 v/o Z	1600°C/45 min	96.7	M, *t*-Z, *m*-Z
MZY20	80 v/o M + 20 v/o Z	1600°C/45 min	95.4	M, *t*-Z, *m*-Z
MZY30	70 v/o M + 30 v/o Z	1600°C/45 min	96.7	M, *t*-Z, *m*-Z
MZY40	60 v/o M + 40 v/o Z	1600°C/45 min	97.5	M, *t*-Z, *m*-Z
MZY50	50 v/o M + 50 v/o Z	1600°C/45 min	97.1	M, *t*-Z, *m*-Z
MZY60	40 v/o M + 60 v/o Z	1600°C/45 min	97.8	M, *t*-Z, *m*-Z
MZY80	20 v/o M + 80 v/o Z	1600°C/45 min	97.7	M, *t*-Z, *m*-Z
Z	100 v/o Z	1600°C/45 min	99.9	*t*-Z, *m*-Z

* M = mullite; Z = 3 mol% Y_2O_3-ZrO_2; *t*-Z = tetragonal ZrO_2; *m*-Z = monoclinic ZrO_2

[#] All samples were fabricated under the pressure of 30 MPa in Ar.

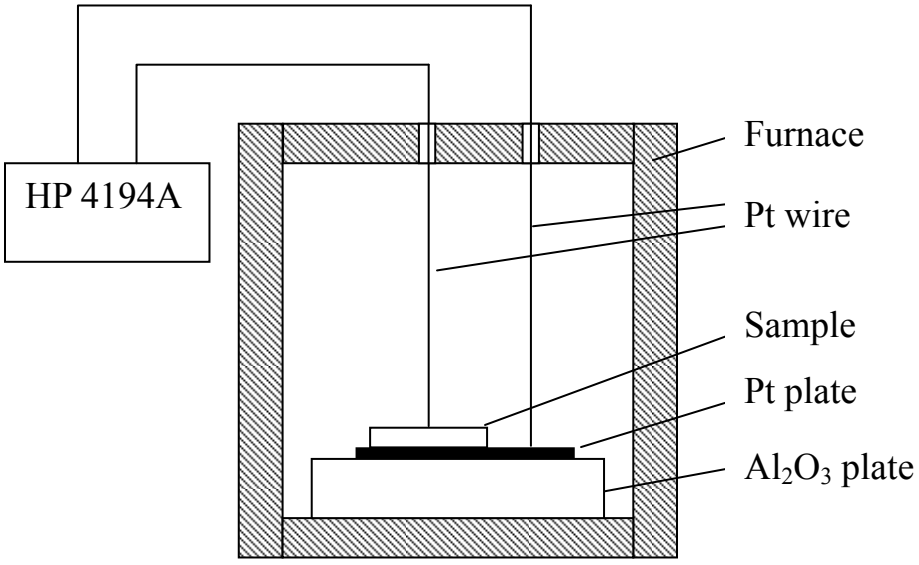

Fig. 3.1 Impedance-measuring system.

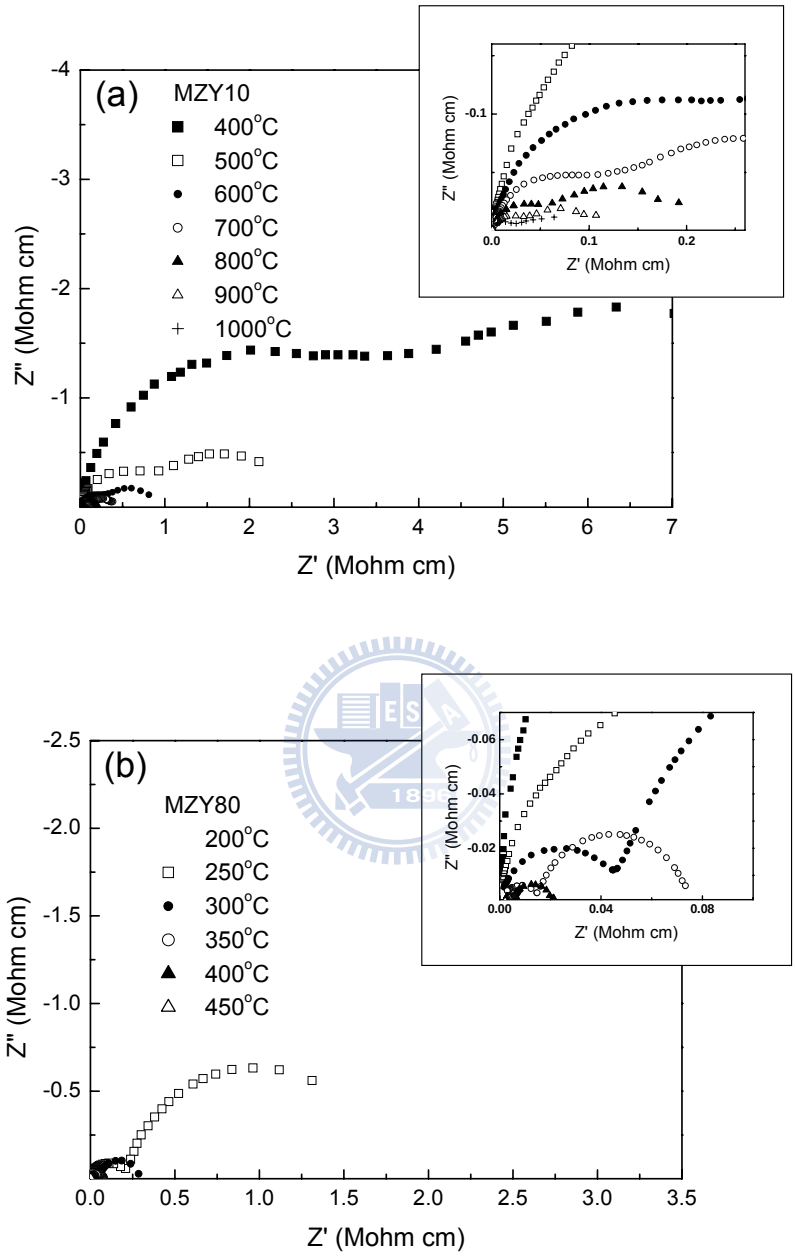

Fig. 3.2 Typical impedance spectra. (a) For MZY10 at temperatures ranging from 400 to 1000°C; (b) For MZY80 at temperatures ranging from 200 to 450°C. The enlarged views at low impedances are shown in the inset.

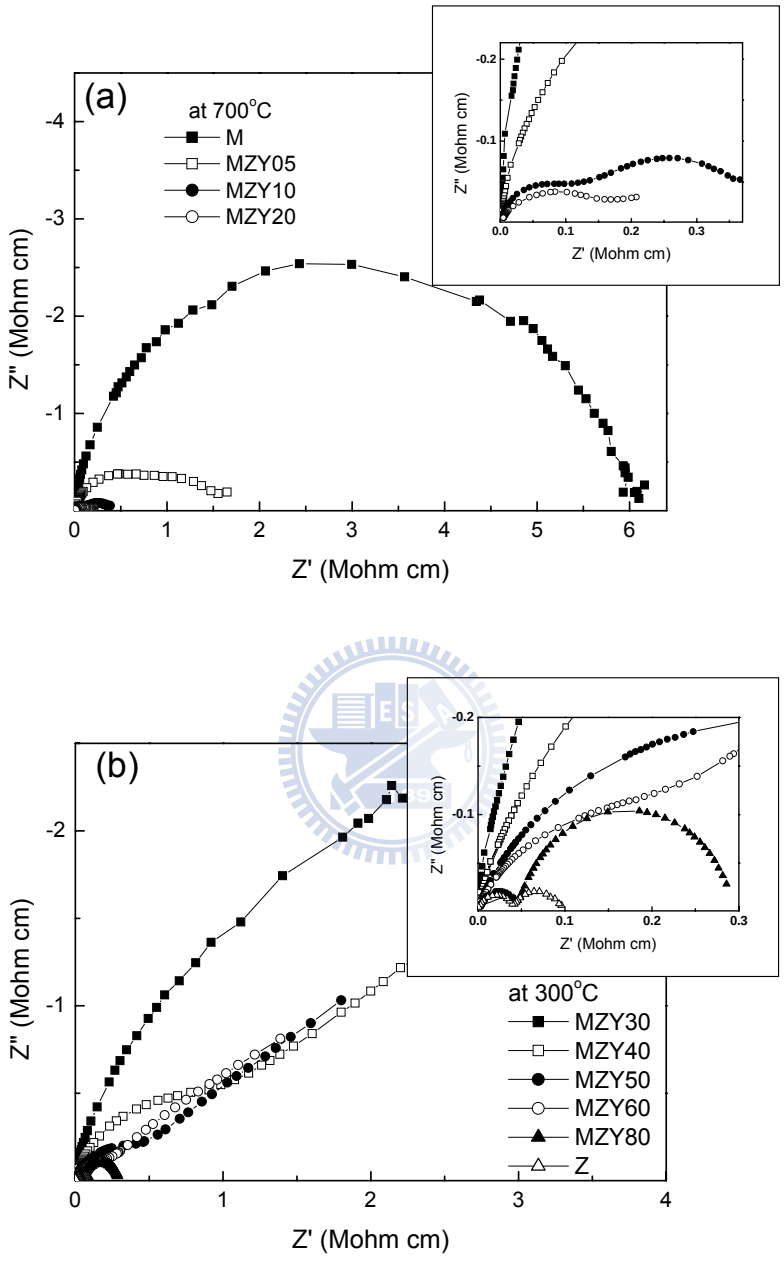

Fig. 3.3 Impedance spectra of the composites with various PSZ contents: (a) M, MZY05, MZY10 and MZY20 at 700°C; (b) MZY30, MZY40, MZY50, MZY60, MZY80 and Z at 300°C. The enlarged views at low impedances are shown in the inset.

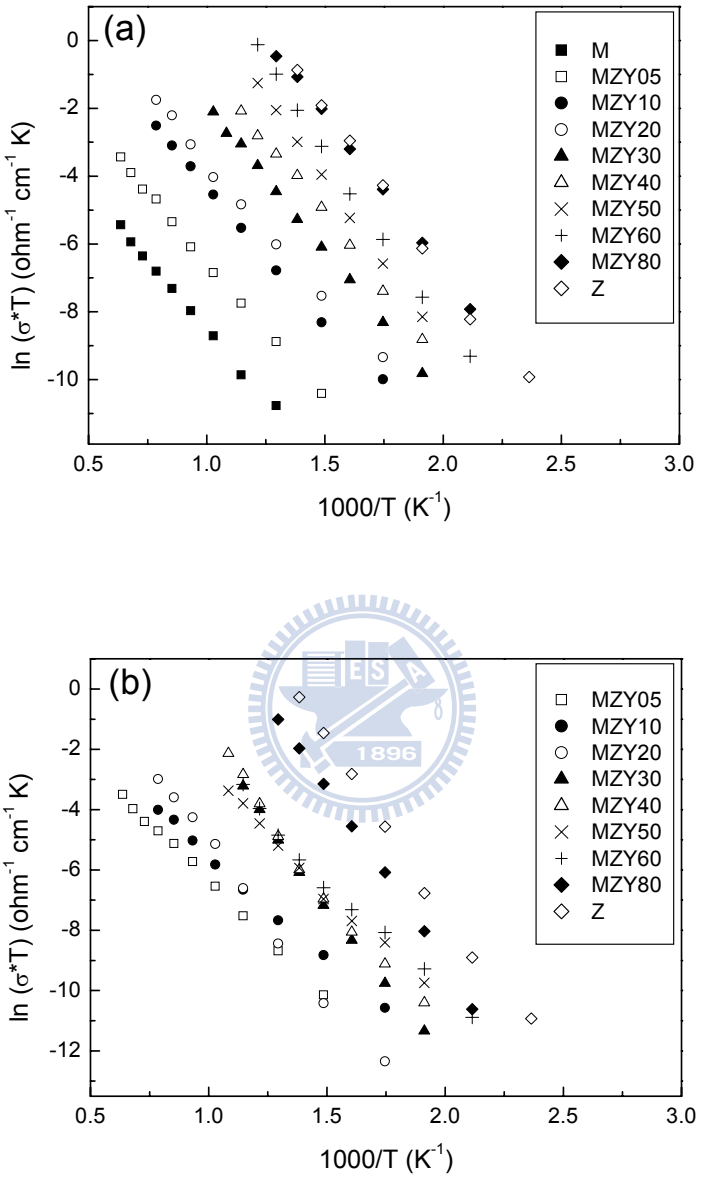

Fig. 3.4 Arrhenius plots of conductivities determined (a) in the high-frequency region; (b) in the low-frequency region of impedance spectra.

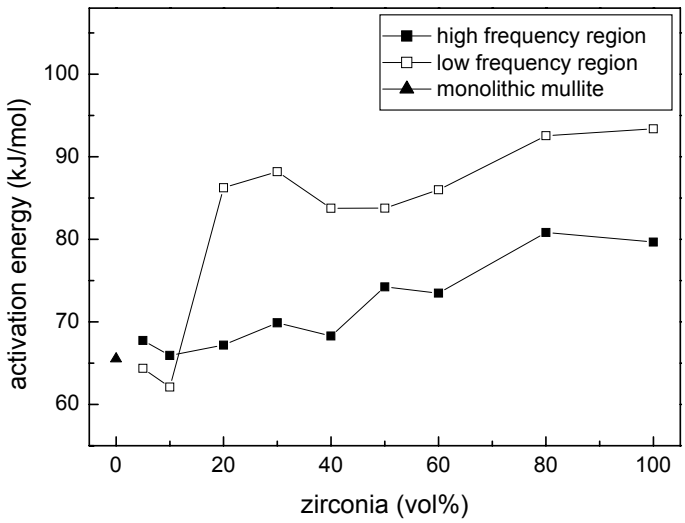

Fig. 3.5 The activation energy versus PSZ content curves of mullite/PSZ composites in the high-frequency and low-frequency regions, respectively, of the impedance spectra.

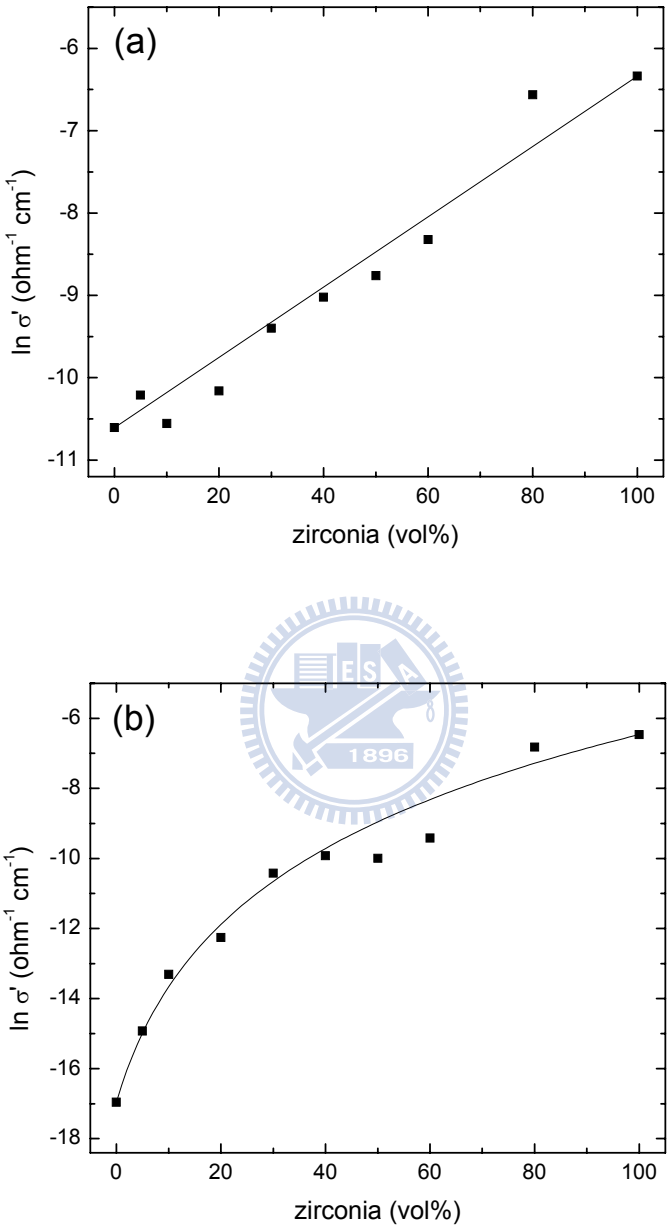

Fig. 3.6 The real part of conductivity versus PSZ content curve at the frequencies of (a) 1 MHz and (b) 1 KHz at 600°C. The fitting lines in (a) and (b) were determined by Lichtenecker's rule and the general mixing equation, respectively.

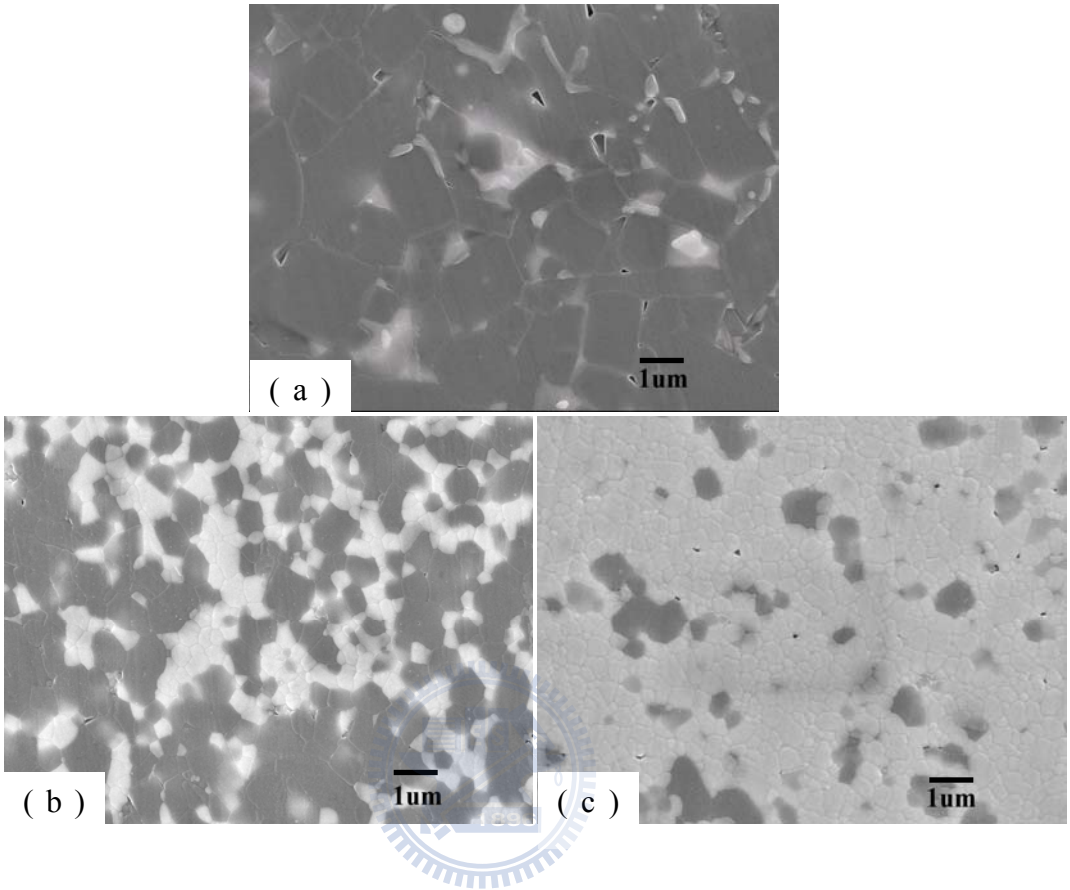

Fig. 3.7 Scanning electron micrographs of mullite/PSZ composites: (a) MZY05; (b) MZY30; (c) MZY80. The dark phase is mullite and the bright phase is PSZ.

Chapter 4

Oxygen Diffusivities and Surface Exchange Coefficients in Porous Mullite/Zirconia Composites Measured by the Conductivity Relaxation Method

4.1 Introduction

Mullite is a frequently used material for applications at high temperatures due to its advantageous properties, including good creep resistance, excellent chemical stability, and suitable high-temperature strength.[1] In addition, mullite is a potential substrate material because it has a favorable dielectric constant and thermal expansion coefficient.[58] To further improve its mechanical properties (e.g., fracture toughness), ZrO_2 particles and/or SiC whiskers have been incorporated in mullite, as indicated in previous studies.[5, 9, 59, 60]

One can modify the properties of composite materials by combining two or more components. The properties of composites are highly dependent upon the size, shape and content of the individual components. Previous studies[57, 61] investigated the oxygen diffusivities and electrical conductivities of mullite/PSZ composites with various PSZ contents. The percolation phenomenon for oxygen diffusion in mullite/PSZ composites was observed at 30-40 vol% PSZ, while no such a phenomenon was observed for electrical conduction.[61] The electrical conductivities of mullite/PSZ composites followed Lichtenecker's rule at high frequencies and the general mixing equation at low frequencies.

Recently, the mechanical properties of porous mullite/ZrO_2 composites have been investigated.[62, 63] Haslam and Lange[62] developed a processing method to strengthen porous mullite/ZrO_2 composites without shrinkage using evaporation/condensation sintering in an HCl atmosphere. Latella and Mehrtens[63] indicated that the mullite/ZrO_2 composites with 62% porosity showed no strength degradation at temperatures ranging from 25 to 1200^{o}C. Because porous composites could be used in hot gas filtration environments, the influence of ZrO_2 content on diffusion and/or surface exchange rate in porous mullite/ZrO_2 composites is an important subject.

To date, little research has been conducted on the character of mass transfer in porous mullite/ZrO_2 composites. In a previous study,[64] Ganeshananthan and Virkar measured the oxygen surface exchange coefficients of porous $La_{0.6}Sr_{0.4}CoO_{3-\delta}$ using the conductivity relaxation method. In this study, the conductivity relaxation method was used to measure the diffusivities and surface exchange coefficients of porous mullite/PSZ composites with various PSZ contents. The effects of PSZ content and oxygen partial pressure on the diffusivities and surface exchange coefficients of porous mullite/PSZ composites were explored.

4.2 Experimental Procedures

Based upon a previous study on the percolation phenomenon, mullite/PSZ composites containing more than 40 vol% PSZ were defined as "high-PSZ composites"; otherwise, the composites were categorized as "low-PSZ composites."

The composites in this study were fabricated by sintering mixtures of mullite (KM-mullite, 71.86 wt% Al_2O_3, 28.07 wt% SiO_2, 0.03 wt% Fe_2O_3, 0.03 wt% NaO_2 and 0.01 wt% MgO_2, 0.2 μm on average, Kyoritsu Ceramic Materials Co., Nagoya, Japan), 3 mol% Y_2O_3-stabilized ZrO_2 or 3Y-ZrO_2 powder (TZ-3Y, 94.75 wt% ZrO_2, 5.21 wt% Y_2O_3, 0.005 wt% Al_2O_3, 0.005 wt% SiO_2, 0.002 wt% Fe_2O_3 and 0.022 wt% NaO_2, 0.3 μm on average, Toyo Soda Mfg., Co., Tokyo, Japan), and carbon (Vulcan XC72, 0.03 μm on average, Cabot Co., Billerica, MA), wherein 30 vol% carbon was used as the pore-forming agent.

The starting powders were first dispersed in alcohol. The pH value was adjusted to 10 using NH_4OH as an electrolyte, and then the powder mixtures were dried on a hot plate. Subsequently, they were uniaxially pressed at 63 MPa for a few minutes. The cold-pressed samples were heated to burn out carbon at 600°C for 30 min and then sintered at 1200-1550°C for 2-3 h depending upon the composition of the powder mixture.

The densities of the sintered bodies were determined by the Archimedes method using de-ionized water as an immersing medium, and the relative densities were then calculated. The designations, compositions, sintering conditions, and relative densities of these composites are listed in Table 4.1. The sintered composites were cut into pieces about 3.5 × 3.5 × 0.8 mm in size. Samples were ground and polished with a precision polishing machine (Model Minimet 1000, Buehler Ltd, Lake Bluff, IL) using standard procedures as described previously.[57]

The conductivity relaxation method was used to measure the electrical

resistivities of bulk samples under different oxygen partial pressures. Figure 4.1 shows a schematic diagram of the conductivity-measuring system. The specimen together with two Pt electrodes was clipped by two plates of Al_2O_3. After being connected to an electric potentiometer, the specimen was placed in an Al_2O_3 tube furnace. The measuring temperatures were less than the sintering temperature by at least 200°C to avoid densification during the measurements. When the electric conductivity was saturated at a certain oxygen partial pressure (Po_2^1), a gas mixture with a decreased oxygen partial pressure (Po_2^2) was introduced into the chamber. While the oxygen partial pressure changed from Po_2^1 to Po_2^2, the variation of electrical resistance was recorded with a multimeter (Model 2000, Keithley Instruments Inc, Cleveland, OH). This procedure was repeated using a stepwise decrease in the oxygen partial pressure after the electric conductivity was saturated again.

It was noted that when the ratio of initial to final Po_2 is larger than 20, linear exchange kinetics are no longer valid.[65] Thus, a narrow Po_2 change was conducted to make certain that systematic error in measuring the diffusivities and surface exchange coefficients could be avoided. The oxygen partial pressures chosen in this study were 20.2, 14.1, 10.1, 6.07 and 2.02 kPa in sequence. Variation of the oxygen partial pressure was achieved by different flow rates of oxygen and argon.

4.3 Mathematical Background

Transport of oxygen ions in a porous sample consists of two possible rate-controlling processes in series: the surface exchange reaction at the

gas/solid interface and ionic diffusion through the bulk. If the oxygen concentration at any cross-section is kept constant, i.e., the flux into the cross-section is equal to the flux out of the cross-section, a steady state is reached. When the oxygen partial pressure is changed in a steady state system, the variation of oxygen concentration in the solid with time can be correlated with the rates of bulk diffusion and surface exchange by the following equation:[66]

$$\frac{M_t}{M_\infty} = 1 - \sum_{n=1}^{\infty} \frac{2L^2 \exp\left(-\frac{t}{\tau_n}\right)}{\beta_n^2\left(\beta_n^2 + L^2 + L\right)} \tag{4.1}$$

where M_t is the total amount of ions that entered (or left) the sample in time t, M_∞ is the total amount of ions that entered (or left) the sample after an infinite time, τ_n is the relaxation time, and β_n are the positive roots of the following equation:

$$\beta \tan \beta = L = \frac{l \cdot \alpha}{D} \tag{4.2}$$

where α is the surface exchange coefficient, D is the diffusivity, and l is the half thickness of the membrane. As a result, the relaxation time τ_n can be expressed as follows:

$$\tau_n = \frac{l^2}{D \cdot \beta_n^2} \tag{4.3}$$

Either bulk diffusion or surface exchange reactions can be a rate-limiting

step in the relaxation process, and the ratio of diffusivity to the surface exchange coefficient is defined as the characteristic length (L_c).[67, 68] When the thickness of the membrane is much larger than the characteristic length, diffusion will govern the relaxation process. In such a case, where diffusion controls ionic transport, Eqn. (4.1) can be expressed as

$$\frac{M_t}{M_\infty} = 1 - \sum_{n=0}^{\infty} \frac{8}{(2n+1)^2 \pi^2} \exp\left[\frac{-D(2n+1)^2 \pi^2 t}{4l^2}\right] \tag{4.4}$$

In contrast, when the thickness of the membrane is much smaller than the characteristic length, the relaxation process is mainly dominated by the surface exchange reaction. In such a case, where surface exchange controls ionic transport, Eqn. (4.1) can be simplified as

$$\frac{M_t}{M_\infty} = 1 - \exp\left(-\frac{\alpha \cdot t}{l}\right) \tag{4.5}$$

The equations mentioned above for the relaxation experiment are derived under the assumption of immediate change of oxygen partial pressure. When a relaxation experiment is performed in a large reactor volume or at a relatively high temperature, the time needed to change the oxygen partial pressure cannot be neglected. The relaxation time can be close to the flush time of the reactor volume, and a correction should be used. The flush time correction in a relaxation experiment was presented by den Otter *et al.*[69] Thus, Eqn. (4.1) can be written in terms of the flush time of the reactor volume:

$$g(t) = 1 - \exp\left(-\frac{t}{\tau_f}\right) - \sum_{n=1}^{\infty} \frac{2L^2 \cdot \frac{\tau_n}{\tau_n - \tau_f} \cdot \left[\exp\left(-\frac{t}{\tau_n}\right) - \exp\left(-\frac{t}{\tau_f}\right)\right]}{\beta^2\left(\beta^2 + L^2 + L\right)} \tag{4.6}$$

where $g(t)$ is the normalized conductivity and τ_f is the flush time of the reactor volume or the time needed to flush the reactor volume. Since the relaxation process is controlled by surface exchange, Eqn. (4.6) can be simplified as

$$g(t) = 1 - \exp\left(-\frac{t}{\tau_f}\right) - \frac{\tau}{\tau - \tau_f} \cdot \left[\exp\left(-\frac{t}{\tau}\right) - \exp\left(-\frac{t}{\tau_f}\right)\right] \tag{4.7}$$

where the relaxation time $\tau = l/\alpha$. Additionally, the relationship between the normalized conductivity $g(t)$ and electrical conductivities can be described by

$$g(t) = \frac{\sigma(t) - \sigma(0)}{\sigma(\infty) - \sigma(0)} = \frac{M_t}{M_\infty} \tag{4.8}$$

where $\sigma(0)$ is the initial conductivity and $\sigma(t)$ and $\sigma(\infty)$ are the conductivities at time t and after infinite time, respectively.

4.4 Results and Discussion

4.4.1 Conductivities

Figure 4.2 shows the plot of electrical resistance *versus* time for MZY80 at 750°C while the oxygen partial pressure was changed stepwise from 6.07 to

2.02 kPa. When the system reached an equilibrium state at 6.07 kPa, the resistance approached a certain value. Once the oxygen partial pressure was changed to 2.02 kPa, there was a dramatic increase in resistance and then another equilibrium value was approached. The normalized conductivity $g(t)$ can thus be calculated by setting $\sigma(0)$ and $\sigma(\infty)$ equal to the equilibrium conductivities at 6.07 and 2.02 kPa, respectively, while $\sigma(t)$ is the conductivity at time t after the pressure is changed.

Figure 4.3 displays the relationship between the conductivity and oxygen partial pressure for various composites. The conductivities of these composites increased significantly with PSZ content and increased slightly with oxygen partial pressure. The PSZ content had a larger effect on the conductivity than the oxygen partial pressure did. The slopes of linear log conductivity vs. log oxygen partial pressure curves were between 0.06 and 0.1. For *p*-type electronic conduction, the slope of a logarithmic plot of the electronic conductivity versus oxygen partial pressure was calculated to be 1/4.[70, 71] The fact that the slopes obtained in this study were much lower than 1/4 suggests a significant contribution of ionic conduction.

The relation among the ionic conductivity, electron-hole conductivity and oxygen partial pressure can be expressed by the following equation:[72]

$$\sigma_t = \sigma_i + \sigma_h^0 Po_2^{1/4} \tag{4.9}$$

where σ_t is the total conductivity, σ_i is the ionic conductivity, and σ_h^0 is the electron-hole conductivity at 1 atm oxygen partial pressure. Consequently,

σ_i and σ_h^0 can be determined, respectively, by the intercept and slope of the total conductivity versus $Po_2^{1/4}$ curve. Table 4.2 lists the calculated ionic transport numbers [$t_i = \sigma_i/(\sigma_i+\sigma_h^0)$] of mullite/PSZ composites at various temperatures, which were widely distributed between 0.12 and 0.83. This result indicates that mullite/PSZ composites are mixed ionic and electronic conducting (MIEC) materials.

Figure 4.4 illustrates the relationship between the normalized conductivity and time for mullite/PSZ composites at a fixed temperature with the oxygen partial pressure changed stepwise from 6.07 to 2.02 kPa. Figure 4.4(a) illustrates that the required time for re-equilibration in mullite at 1100°C was about 80,000 s, which was much longer than that of MZY05. Similarly, the re-equilibration time of MZY10 at 1000°C was longer than those of MZY20 and MZY30, as shown in Fig. 4.4(b). In other words, the re-equilibration time of low-PSZ composites decreased with increasing PSZ content. Figure 4.4(c), however, indicates that the re-equilibration times of high-PSZ composites at 750°C were similar, except for MZY40. When the oxygen partial pressure was changed from 6.07 to 2.02 kPa, the re-equilibration time of MZY40 at 750°C was about 700 s, which was about one order of magnitude larger than those of MZY50, MZY60, MZY80 and Z.

4.4.2 Diffusivities and Surface Exchange Coefficients

According to the previous study,[57] a percolation phenomenon was found for the diffusivities and surface exchange coefficients of mullite/PSZ composites. The diffusivities and surface exchange coefficients of low-PSZ composites were close to those of mullite, while the diffusivities and surface exchange coefficients of high-PSZ composites were close to

those of PSZ. The characteristic lengths of low-PSZ composites were about 10^{-8}~10^{-6} m at 1000~1350°C and those of high-PSZ composites were about 10^{-3}~10^{-2} m at 1000~1350°C.

The mean particle size of any component in the porous sample was determined from quantitative image analysis:[73] $\bar{L} = 2V_V / S_V$, where V_V and S_V are the volume fraction of the component and the specific surface area of the porous sample, respectively. The mean particle size ($\bar{L}$) can be regarded as the thickness of the membrane ($2l$), i.e., the parameter l is equal to $\bar{L}/2$. The parameters l of all the composites were estimated to be about $2 \sim 4\times10^{-7}$ m in this study.

Generally speaking, the characteristic lengths of high-PSZ composites were much larger than their corresponding parameters l, and the relaxation processes in high-PSZ composites should be controlled by the surface exchange reaction. On the other hand, the characteristic lengths of low-PSZ composites approximated to their corresponding parameters l, and the relaxation processes in low-PSZ composites can be controlled by both surface exchange and diffusion processes.

Additionally, the flush time of the reactor volume (τ_f) can be given by[69]

$$\tau_f = \frac{V_r}{\Phi_V} \cdot \frac{T_{STP}}{T_r} \tag{4.10}$$

where Φ_V is the flow rate of gas, V_r and T_r are the reactor volume and absolute temperature, respectively, and T_{STP} is room temperature. In this

study, the flow rate of gas was 1 L/min and reactor volume was about 0.390 L. At 750~1300°C, the flush time was estimated to be nearly 6.8~4.4 s, which was quite small and could be neglected with respect to the relaxation time of low-PSZ composites (≈10^4~10^2 s). However, the relaxation time of high-PSZ composites was close to the flush time. Therefore, the relaxation data of low-PSZ composites were fitted by Eqn. (4.1) and those of high-PSZ composites were fitted by Eqn. (4.7), whereby the oxygen diffusivities and surface exchange coefficients of various composites were obtained.

As listed in Table 4.3, the oxygen diffusivities in low-PSZ composites ranged from 1.5 to 913 nm^2/s at 800-1300ºC. It was noted that the diffusivities in low-PSZ composites increased with increasing PSZ content. The diffusivities calculated in this study were higher by 2 to 3 orders of magnitude than those measured by SIMS in the previous study.[57] The tracer diffusivities and chemical diffusivities were measured in the previous study and in this study, respectively. The chemical diffusivity (D_{chem}) and tracer diffusivity (D_{tr}^*) are correlated by the following expression:[74] $D_{chem} = D_{tr}^* \cdot \left(1 + (\mathrm{d}\ln\gamma_i / \mathrm{d}\ln C_i)\right)$, where γ_i and C_i are the activity coefficient and mole fraction of the species i, respectively. The term $(1+\mathrm{dln}\gamma_i/\mathrm{dln}C_i)$ is a thermodynamic factor and is considered as the difference between the chemical diffusivity and tracer diffusivity. Furthermore, the oxygen surface exchange coefficients of low-PSZ composites were in the range of 0.044-8.3 nm/s at 800-1000ºC. As listed in Table 4.4, the oxygen surface exchange coefficients of high-PSZ composites were in the range of 0.66-261 nm/s at 750-850ºC. This indicates that the surface exchange coefficients in low-PSZ composites increased with increasing PSZ content.

However, those in high-PSZ composites (PSZ content ≥ 50 vol%) were all similar. It was noted that oxygen surface exchange decreased with increasing oxygen partial pressure.

4.4.3 Effects of PSZ Content

From the Arrhenius plots of oxygen diffusivities and surface exchange coefficients, the corresponding activation energies can be estimated. Figure 4.5 shows the activation energies of oxygen diffusion and surface exchange *versus* PSZ content for various composites at various oxygen partial pressures. As shown in Fig. 4.5(a), the activation energies of oxygen diffusion decreased with increasing PSZ content and approached the results for low-PSZ composites measured in the previous study.[57] Figure 4.5(b) also illustrates that the activation energies of surface exchange decreased with increasing PSZ content, but the activation energies of surface exchange coefficients in high-PSZ composites approached that for PSZ.

Figure 4.6 shows the effect of PSZ content on the surface exchange coefficient in composites at 800°C. Note that the data for low-PSZ composites were obtained by extrapolation. There was a dramatic change in the surface exchange coefficient at about 40 vol% PSZ. This phenomenon can be explained by percolation theory[23, 24] and effective medium theory.[25] Bruggeman's symmetrical effective medium theory[25] shows a percolation threshold at a conductor volume fraction of 0.33 in a three-dimensional case. The percolation threshold occurred at about 30-40 vol% PSZ, as shown in Fig. 4.6, which approximated the threshold value predicated by Bruggeman's symmetrical effective medium theory. It was noted that the surface exchange coefficient in mullite was much lower than

those in low-PSZ composites (MZY10~MZY30). This was attributed to the fact that the data for mullite were obtained via extrapolation, which has a greater uncertainty in nature.

4.4.4 Effect of Oxygen Partial Pressure

Figure 4.7 displays the relationship between the diffusivities and the oxygen partial pressures for various low-PSZ composites. There was no significant difference in the diffusivities of low-PSZ composites under various oxygen partial pressures. That could be explained by the fact that oxygen diffusion was correlated to the migration of oxygen vacancies, of which the concentration was nearly constant in mullite or PSZ under the various oxygen partial pressures. It is noted that mullite is a non-stoichiometric compound and its chemical formula can be expressed as $Al_2[Al_{2+2x}Si_{2-2x}]O_{10-x}$, where x ($0.17 \leq x \leq 0.59$) is the number of missing oxygen atoms per unit cell. The oxygen vacancies in mullite are formed due to the replacement of Si^{+4} ions by Al^{+3} ions, which can be expressed by the following equation:

$$Al_2O_3 \xrightarrow{SiO_2} 2Al'_{Si} + 3O^{\times}_{O} + V^{\circ\circ}_{O} \tag{4.11}$$

In addition, the formation of oxygen vacancies in Y_2O_3-ZrO_2 can be expressed by

$$Y_2O_3 \xrightarrow{ZrO_2} 2Y'_{Zr} + 3O^{\times}_{o} + V^{\circ\circ}_{O} \tag{4.12}$$

The concentration of oxygen vacancies formed in mullite and PSZ are

extrinsically fixed, and are independent of oxygen partial pressure in the range from 20.2 to 2.02 kPa. Therefore, the diffusivities of low-PSZ composites are independent of oxygen partial pressure.

Figure 4.8 illustrates the curves of the surface exchange coefficient *versus* the oxygen partial pressure for mullite at 1100^{o}C, for low-PSZ composites at 1000^{o}C and for high-PSZ composites at 800^{o}C, respectively. The surface exchange coefficients of mullite, MZY20, MZY30 and high-PSZ composites (except MZY05 and MZY10) decreased with increasing oxygen partial pressure. In previous studies, a similar trend was reported between the surface exchange coefficient and oxygen partial pressure in yttria-doped ceria (YDC), yttia-stabilized zirconia (YSZ) or gadolinia-doped ceria (GDC).[75, 76] Horita *et al*.[75] reported that there was a log-linear relationship between the surface exchange coefficient and oxygen partial pressure measured by SIMS in YDC and YSZ with a slope of about -1/20. Karthikeyan *et al*.[76] measured the surface exchange coefficient in thin film GDC using the electrical conductivity relaxation method. They claimed that the limitation to the surface exchange rate of oxygen resulted from a reduction in carrier concentration due to the segregation of Gd in near-surface regions.

4.4.5 Rate-Determining Mechanisms of Oxygen Surface Exchange

Horita *et al*.[75] reported that the rate-determining step for an oxygen surface exchange reaction in YDC and YSZ was the adsorption of oxygen at the gas/solid interface. However, Sirman *et al*.[77] indicated that the rate-limiting step for oxygen surface exchange might be the charge-transfer process in GDC and other fluorite materials. During the conductivity relaxation

experiment, the surface exchange rate depended on the following reaction taking place at the gas/solid interface:[78, 79]

$$\frac{1}{2}O_{2(g)} + 2e^- + V_O^{\circ\circ} \rightarrow O_O^{\times} \tag{4.13}$$

The reaction of Eqn. (4.13) can be separated into several steps as follows:

$$\frac{1}{2}O_{2(g)} \rightarrow \frac{1}{2}O_{2(g,\,Pt\text{-}pores)} \quad \text{(gas phase diffusion)} \tag{4.14}$$

$$\frac{1}{2}O_{2(g,\,Pt\text{-}pores)} + S_{ad} \rightarrow O_{ad} \quad \text{(adsorption and dissociation)} \tag{4.15}$$

$$O_{ad} \rightarrow O_{ad(reaction\ site)} \quad \text{(surface diffusion)} \tag{4.16}$$

$$O_{ad(reaction\ site)} + 2e^- + V_O^{\circ\circ} \rightarrow O_O^{\times} \quad \text{(charge-transfer reaction)} \tag{4.17}$$

The gas phase diffusion coefficient within the O_2/Ar mixing gas can be calculated by the Chapman-Enskog equation:[80]

$$D_m = \frac{1.86 \cdot 10^{-3} T^{3/2} (1/M_1 + 1/M_2)^{1/2}}{p\sigma_{12}{}^2 \Omega} \tag{4.18}$$

where T is temperature (K), M_1 and M_2 are the molecular weight of gas 1 and gas 2, p is the pressure (atm), σ_{12} is the collision diameter (Å), Ω is the nondimensional collision integral, and the unit of D_m is cm^2/s. When the

mean free path of the gas is greater than the pore diameter, Knudsen diffusion should be considered. The Knudsen diffusion coefficient, D_{Kn}, is given by

$$D_{Kn} = 4850 \cdot d \cdot \sqrt{\frac{T}{M}} \tag{4.19}$$

where d is the pore diameter (cm), T is temperature, M is the molecular weight and the unit of D_{Kn} is cm^2/s. The effective diffusion coefficient, D_{eff}, of the gas through porous samples can be estimated by

$$D_{eff} = f_v \frac{D_p}{\tau} \tag{4.20}$$

where f_v is the void fraction, τ is the tortuosity (range between 2 and 6, averaging about 3), and D_p is the diffusion coefficient within the pores (i.e., D_m for mixing gas diffusion and D_{Kn} for Knudsen diffusion).

The calculated effective diffusion coefficients in the O_2-Ar mixing gas in this study were between 0.23 and 0.52 cm^2/s and those of Knudsen diffusion were between 0.25 and 0.55 cm^2/s. It was concluded that the effective diffusion coefficient for the mixing gas was very close to Knudsen diffusivities. However, they were much larger than the oxygen diffusion coefficients in those porous samples. Hence, gas phase diffusion in porous samples could not be the rate determining step (RDS).

In the previous studies[81, 82] on the electrode reaction at the interface between

Pt and yttria-doped zirconia, the RDS was the dissociative adsorption of oxygen on the Pt surface with an activation energy of about 154 kJ/mol for $T \leq 500^{o}C$, while it was the surface diffusion of O_{ad} atoms on the Pt surface to the Pt/zirconia contact with an activation energy of about 171 kJ/mol for $T \geq 600^{o}C$. Additionally, Yoon *et al.*[79] indicated that the RDS was the migration of oxygen vacancies to the triple phase boundary line at temperatures above $800^{o}C$ and low oxygen pressures, based on the assumption that the charge-transfer reactions and adsorption and dissociation process are fast.

The equilibrium constant of Eqn. (4.13) is expressed by the following equation:

$$K = [V_O^{\circ\circ}][e']^2 P_{O2}^{1/2} \tag{4.21}$$

When the concentration of oxygen vacancies in mullite [Eqn. (4.11)] is higher than that of oxygen vacancies formed on the surface [Eqn. (4.13)] (thermodynamical formation),[48] the relation to the defect concentration obtained from Eqn. (4.11) can be described as follows:

$$[V_O^{\circ\circ}] = \frac{1}{2}[Al_{Si}^{'}] \tag{4.22}$$

Combining Eqn. (4.21) with Eqn. (4.22) results in

$$[e'] = (2K)^{1/2}[Al_{Si}^{'}]^{-1/2} P_{O2}^{-1/4} \tag{4.23}$$

Similarly, when the concentration of oxygen vacancies in PSZ is determined extrinsically by $[Y'_{Zr}]$, the relation to defect concentrations obtained from Eqn. (4.12) can be described as follows:

$$[V_O^{\circ\circ}] = \frac{1}{2}[Y'_{Zr}] \tag{4.24}$$

Combining Eqn. (4.21) with Eqn. (4.24) results in

$$[e'] = (2K)^{1/2}[Y'_{Zr}]^{-1/2} P_{O2}^{-1/4} \tag{4.25}$$

The concentration of electronic defects in mullite and PSZ are proportional to $Po_2^{-1/4}$. When the surface exchange coefficient is dominated by the charge-transport process, the slope of -1/4 for the logα-logPo_2 plot can be expected. Seeing that the slopes of the logα-logPo_2 plots for mullite/PSZ composites deviated slightly from -1/4, as shown in Fig. 4.8, it was inferred that the surface exchange rate was dependent on the concentration of electrons.

4.5 Conclusions

1. Oxygen diffusivities and surface exchange coefficients in porous low-PSZ composites can be measured using the conductivity relaxation method. However, the oxygen diffusivities in porous high-PSZ composites could not be determined because of the predominant surface exchange reaction.

2. The surface exchange coefficients in porous high-PSZ composites can be solely determined without respect to diffusivities, because the surface exchange reaction was the rate-limiting step for porous high-PSZ composites.
3. Oxygen diffusivities and surface exchange coefficients in low-PSZ composites increased with PSZ content, while the surface exchange coefficients in high-PSZ composites stayed approximately constant.
4. The surface exchange coefficients in porous mullite/PSZ composites exhibited the percolation phenomenon with a threshold approximately at 40 vol% PSZ.
5. The oxygen diffusivities in porous low-PSZ composites were independent of the oxygen partial pressure at 2.02 kPa $\leq P_{O_2} \leq$ 20.2 kPa. This implied that oxygen diffusion was related to the migration of oxygen vacancies since the concentration of vacancies was independent of the oxygen partial pressure.
6. The surface exchange coefficients in porous high-PSZ composites decreased with increasing oxygen partial pressure with the slopes of the logα-logP_{O_2} plots slightly deviating from -1/4. It was thus inferred that the surface exchange rate was dependent on the concentration of electrons.

Table 4.1 Designations, compositions, sintering conditions, and relative densities of various mullite/PSZ composites

Designation	Composition*	Sintering Conditions	Relative Density (%)
M	(100 v/o M + 0 v/o Z) + 30 v/o C	1550°C/3hr/air	46.3
MZY05	(95 v/o M + 5 v/o Z) + 30 v/o C	1400°C/3hr/air	44.9
MZY10	(90 v/o M + 10 v/o Z) + 30 v/o C	1400°C/3hr/air	45.2
MZY20	(80 v/o M + 20 v/o Z) + 30 v/o C	1400°C/3hr/air	47.5
MZY30	(70 v/o M + 30 v/o Z) + 30 v/o C	1350°C/2hr/air	46.8
MZY40	(60 v/o M + 40 v/o Z) + 30 v/o C	1350°C/2hr/air	50.9
MZY50	(50 v/o M + 50 v/o Z) + 30 v/o C	1300°C/2hr/air	44.5
MZY60	(40 v/o M + 60 v/o Z) + 30 v/o C	1300°C/2hr/air	51.8
MZY80	(20 v/o M + 80 v/o Z) + 30 v/o C	1200°C/2hr/air	43.1
Z	(0 v/o M + 100 v/o Z) + 30 v/o C	1200°C/2hr/air	47.5

* M = mullite; Z = 3 mol% Y_2O_3-ZrO_2 (3Y-PSZ); C = carbon. The carbon content (30 vol%) is based on the individual powder mixtures, while the contents included in parentheses are based on the final sintered composites.

Table 4.2 Ionic transport numbers of mullite/PSZ composites at various temperatures

	Ionic transport numbers							
Composites	750ºC	800ºC	850ºC	900ºC	1000ºC	1100ºC	1200ºC	1300ºC
M	-	-	-	-	-	0.53	0.35	0.31
MZY05	-	-	-	-	0.60	0.65	0.54	-
MZY10	-	-	-	0.53	0.72	0.83	-	-
MZY20	-	-	-	0.41	0.57	0.67	-	-
MZY30	-	0.26	-	0.52	0.62	-	-	-
MZY40	0.61	0.61	0.48	-	-	-	-	-
MZY50	0.54	0.46	0.40	-	-	-	-	-
MZY60	0.17	0.20	0.12	-	-	-	-	-
MZY80	0.12	0.13	0.14	-	-	-	-	-
Z	0.68	0.48	0.41	-	-	-	-	-

Table 4.3 Oxygen diffusivities and surface exchange coefficients of low-PSZ composites at various temperatures and oxygen partial pressures

		6.07→2.02 (kPa)	10.1→6.07 (kPa)	14.1→10.1 (kPa)	20.2→14.1 (kPa)
M					
1100 °C	D(nm^2/s)	1.7	1.5	3.6	3.9
	α (nm/s)	0.078	0.077	0.044	0.045
1200 °C	D(nm^2/s)	27	23	29	16
	α (nm/s)	0.39	0.52	0.23	0.56
1300 °C	D(nm^2/s)	86	110	103	88
	α (nm/s)	1.6	4.2	1.9	1.7
MZY05					
1000 °C	D(nm^2/s)	3.5	4.7	4.4	7.9
	α (nm/s)	0.15	0.10	0.16	0.20
1100 °C	D(nm^2/s)	43	24	35	40
	α (nm/s)	0.33	0.17	0.37	0.45
1200 °C	D(nm^2/s)	62	90	72	101
	α (nm/s)	0.99	0.87	1.2	1.5
MZY10					
900 °C	D(nm^2/s)	18	24	12	20
	α (nm/s)	0.42	0.23	0.29	0.21
1000 °C	D(nm^2/s)	93	122	132	113
	α (nm/s)	0.68	0.49	0.93	0.81
1100 °C	D(nm^2/s)	913	745	527	481
	α (nm/s)	4.2	3.4	3.1	2.2
MZY20					
900 °C	D(nm^2/s)	20	40	26	50
	α (nm/s)	0.43	0.89	0.55	0.84
1000 °C	D(nm^2/s)	116	278	272	258
	α (nm/s)	3.6	2.6	2.0	1.9
1100 °C	D(nm^2/s)	594	586	696	888
	α (nm/s)	6.8	7.5	11	5.4
MZY30					
800 °C	D(nm^2/s)	19	18	15	24
	α (nm/s)	0.25	0.21	0.12	0.17
900 °C	D(nm^2/s)	97	43	55	60
	α (nm/s)	0.96	0.39	0.46	0.34
1000 °C	D(nm^2/s)	358	566	241	410
	α (nm/s)	8.3	3.9	1.7	2.3

Table 4.4 Oxygen surface exchange coefficients of high-PSZ composites at various temperatures and oxygen partial pressures

		6.07→2.02 (kPa)	10.1→6.07 (kPa)	14.1→10.1 (kPa)	20.2→14.1 (kPa)
MZY40					
750 °C	α (nm/s)	0.80	0.76	0.66	0.67
800 °C	α (nm/s)	1.3	1.3	1.1	1.0
850 °C	α (nm/s)	2.0	1.8	1.8	1.7
MZY50					
750 °C	α (nm/s)	51	32	28	15
800 °C	α (nm/s)	137	71	46	36
850 °C	α (nm/s)	147	114	104	44
MZY60					
750 °C	α (nm/s)	48	33	30	24
800 °C	α (nm/s)	150	96	58	40
850 °C	α (nm/s)	160	108	85	65
MZY80					
750 °C	α (nm/s)	74	63	46	20
800 °C	α (nm/s)	181	102	69	37
850 °C	α (nm/s)	239	221	138	56
Z					
750 °C	α (nm/s)	94	79	64	66
800 °C	α (nm/s)	156	168	107	65
850 °C	α (nm/s)	261	217	196	212

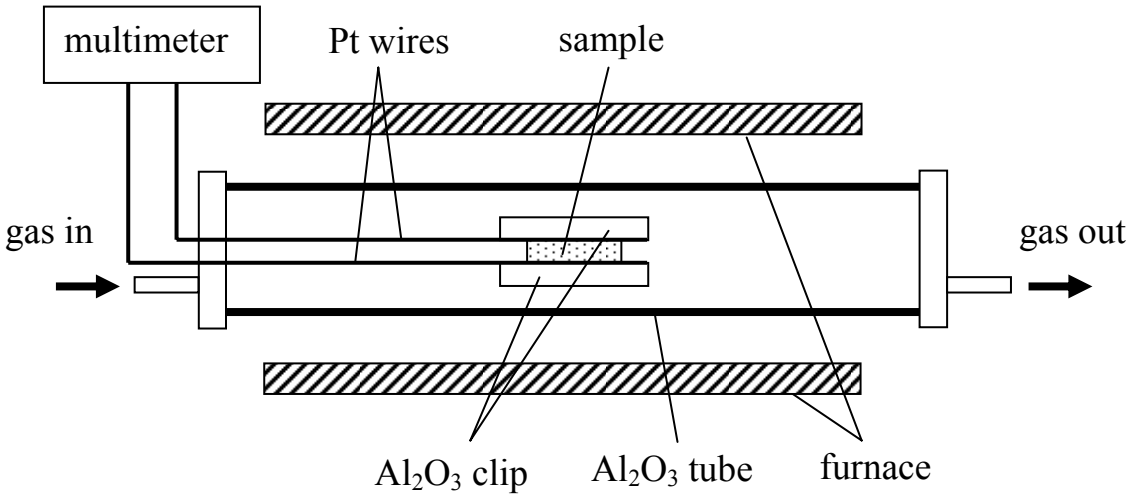

Fig. 4.1 Schematic diagram of the conductivity-measuring system

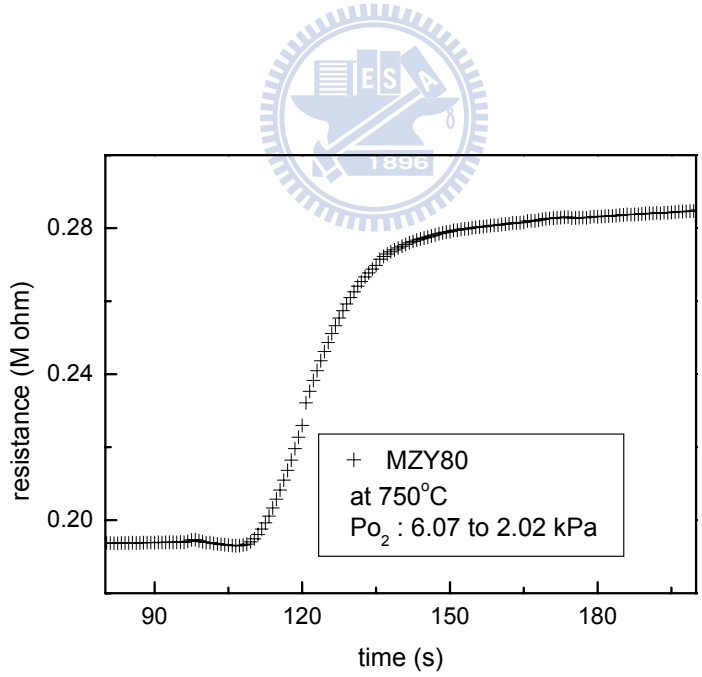

Fig. 4.2 Electrical resistance as a function of time for MZY80 at 750°C when the oxygen partial pressure was changed stepwise from 6.07 to 2.02 kPa .

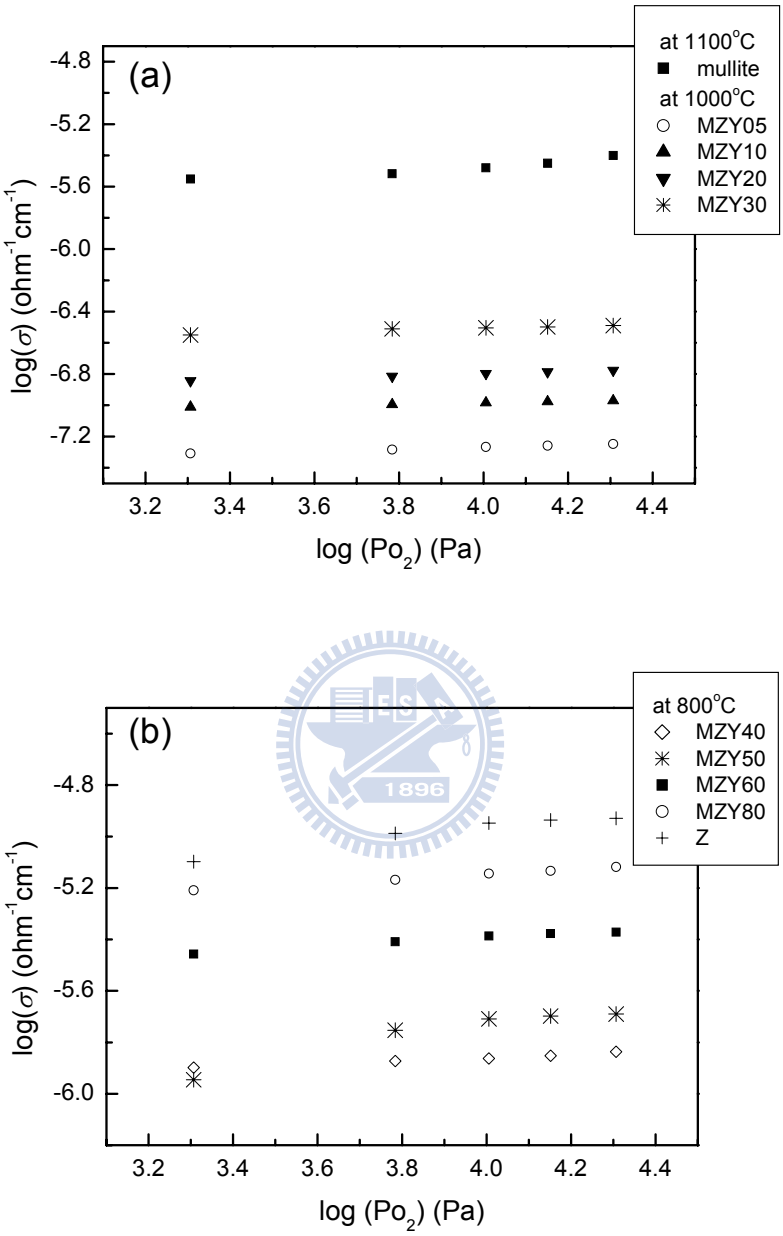

Fig. 4.3 Conductivity vs. oxygen partial pressure curves for (a) mullite at 1100°C and low-PSZ composites at 1000°C; (b) high-PSZ composites at 800°C.

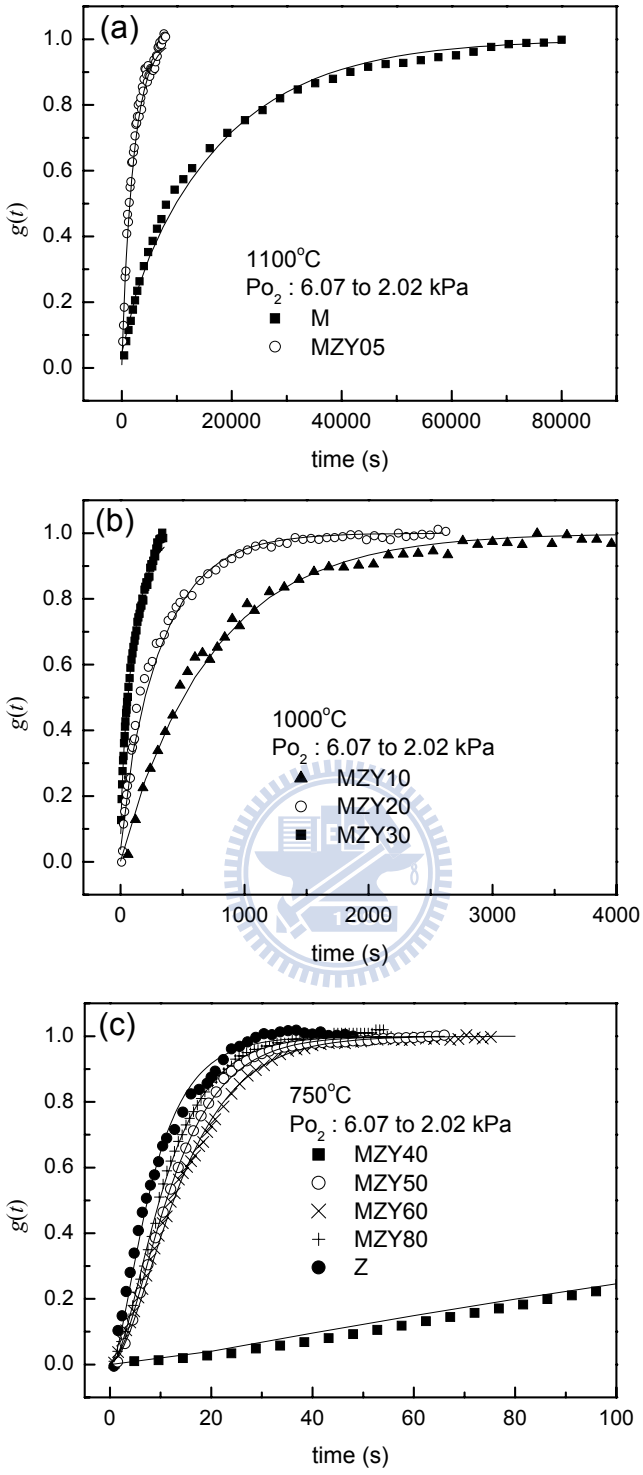

Fig. 4.4 Plots of the normalized conductivity $g(t)$ versus time for (a) M and MZY05 at 1100°C; (b) MZY10, MZY20, and MZY30 at 1000°C; (c) MZY40, MZY50, MZY60, MZY80 and Z at 750°C with the oxygen partial pressure switched from 6.07 to 2.02 kPa . The fitting lines in (a) and (b) were based on Eqn. (4.1), and those in (c) were based on Eqn. (4.7).

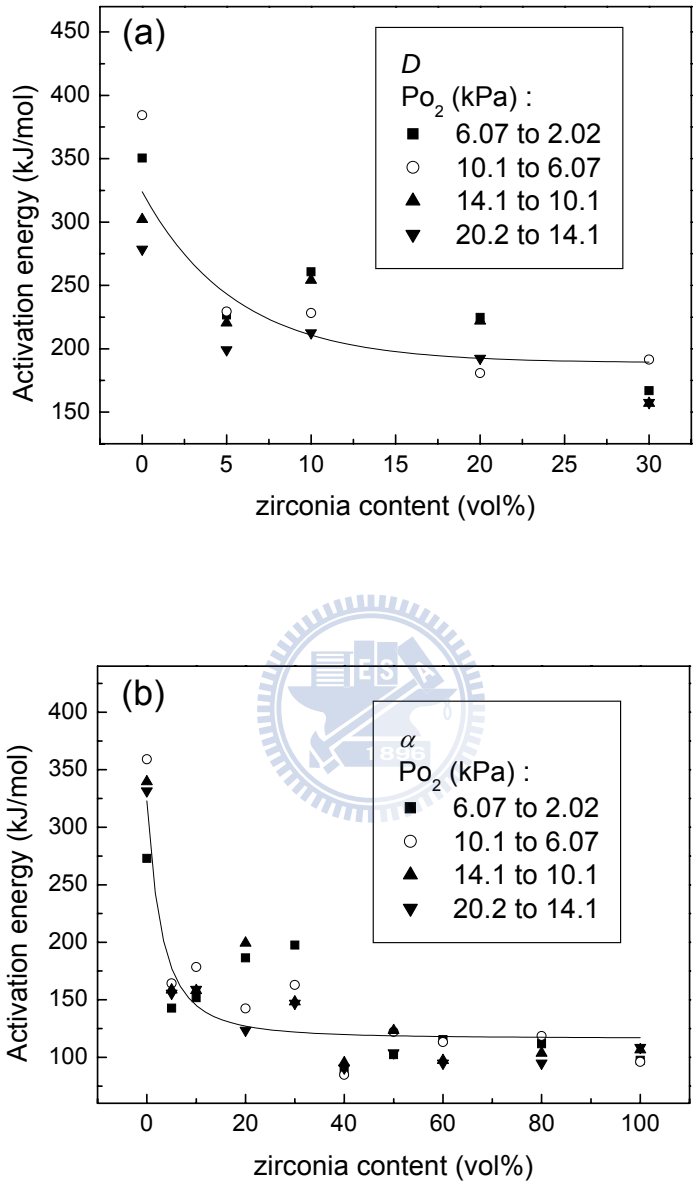

Fig. 4.5 The plot of the activation energy versus PSZ content in mullite/PSZ composites for (a) diffusion coefficients and (b) surface exchange coefficients.

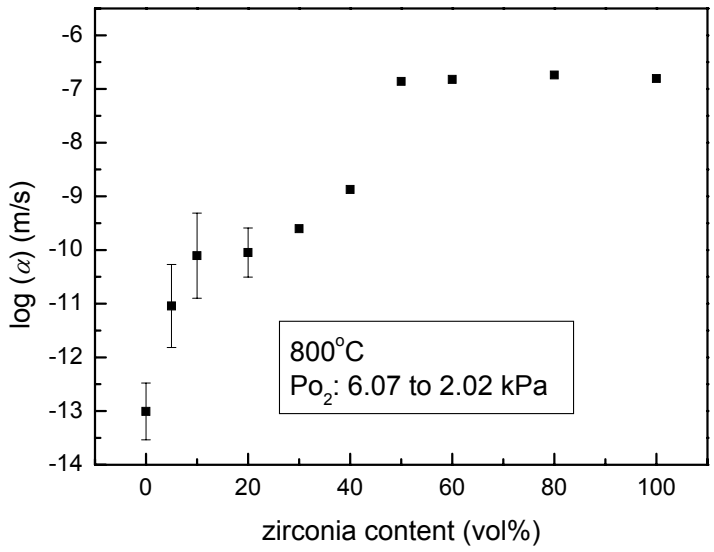

Fig. 4.6 The relationship between surface exchange coefficient and PSZ content at 800°C. The data of low-PSZ composites with error bars were obtained from the extrapolation.

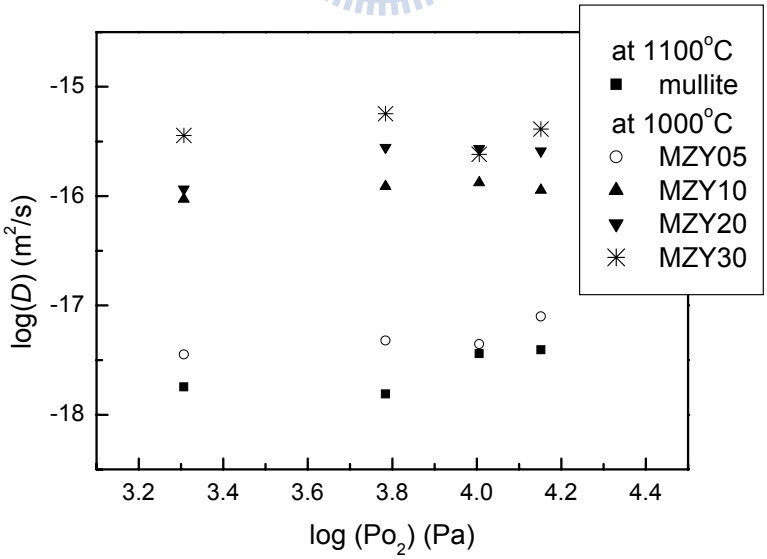

Fig. 4.7 The diffusivity vs. oxygen partial pressure curves for monolithic mullite at 1100°C and low-PSZ composites at 1000°C.

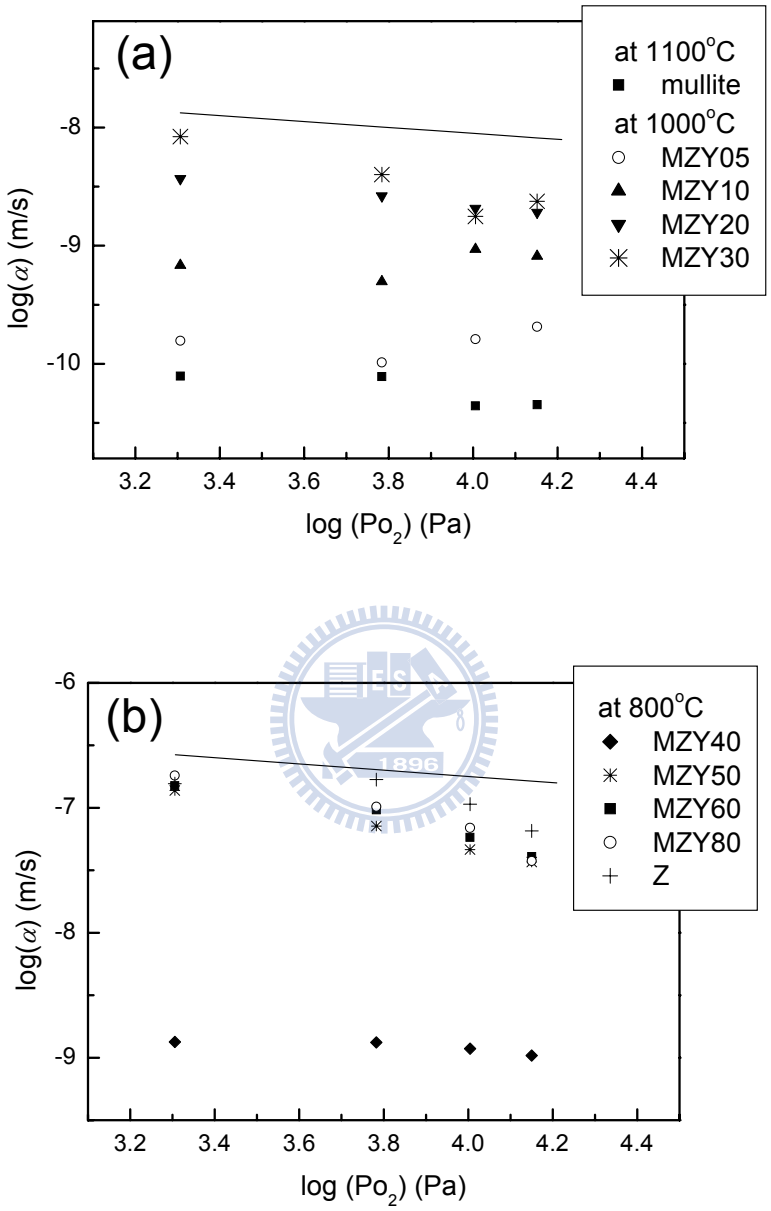

Fig. 4.8 The surface exchange coefficient vs. oxygen partial pressure curves for (a) mullite at 1100°C and low-PSZ composites at 1000°C; (b) high-PSZ composites at 800°C. A slope of -1/4 is presented with the solid line.

Chapter 5

Summary

Mullite has become a potential material for advanced structural and functional ceramic. There are wide applications for mullite-based composites in industry, for example refractory materials, high-temperature engineering materials, electronic packaging materials, optical materials, etc.

In the other respect, aliovalent oxide doped ZrO_2 has been attracted a great deal of attention for engineering applications such high temperature solid oxide fuel cells, oxygen sensors, and electrochemical oxygen pumps. Oxygen vacancies cause high oxygen-ion mobility in fully or partially stabilized ZrO_2, since the vacancy mechanism is a predominant diffusion process for oxygen in ZrO_2.

In order to enhance the mechanical properties of mullite, various mullite-matrix composites have been studied since the stress-induced phase transformation toughening plays a major toughening mechanism in ZrO_2-toughened mullite composite.

In this study, dense and porous mullite/PSZ composites with various mullite:PSZ ratio were prepared by either hot-pressing or pressureless sintering. Oxygen diffusivities and surface exchange coefficients in dense samples were measured by $^{18}O/^{16}O$ isotope exchange method and secondary ion mass spectrometry. Electrical conductivities in dense samples were measured by AC impedance spectroscopy. Oxygen diffusivities and

surface exchange coefficients in various porous mullite/PSZ composites were measured at oxygen partial pressures ranging from 20.2 to 2.02 kPa using the conductivity relaxation method.

Oxygen diffusivities in dense mullite/PSZ composites exhibited a wide range of values from 10^{-21} to 10^{-10} m^2/s at temperatures between 1000 and 1350°C. The oxygen diffusivities in these mullite/PSZ composites exhibited a threshold of PSZ content at between 30 and 40 vol%. The high-PSZ composites showed relatively high oxygen diffusivities, close to the oxygen diffusivity in PSZ. Correspondingly, the low-PSZ composites showed relatively small oxygen diffusivities, close to the oxygen diffusivity in mullite.

There was also a clear tendency that the activation energies of oxygen diffusion in dense mullite/PSZ composites decrease with increasing PSZ contents. The activation energies of oxygen diffusion in high-PSZ composites were close to that of PSZ, while those of low-PSZ composites approached that of mullite. The extreme difference in oxygen diffusivities between low-PSZ and high-PSZ composites was explained by the microstructural features of the composites. In the high-PSZ composites, the relatively large oxygen diffusivities were attributed to the interconnected PSZ channels, which provided a fast diffusion path for oxygen.

The impedance spectra of monolithic PSZ and mullite/PSZ composites showed two semicircles because of the contributions from grains and grain boundaries, while those of monolithic mullite had one semicircle due to the predominant contribution from grains. The conductivities of mullite/PSZ

composites increased with the PSZ content, but no percolation relationship was observed. While the conductivities of various composites at 1 MHz were fitted by Lichtenecker's rule, the general mixing equation could be applied to the conductivities measured at 1 kHz.

The activation energies of electrical conduction for dense mullite/PSZ composites were very different in the high-frequency and low-frequency regions, depending on the PSZ content. The activation energies of grain conductivities in mullite and PSZ were about 65 and 79 kJ/mol, respectively, while those in mullite/PSZ composites were calculated in between these two end values. Furthermore, the activation energies sharply increased at 10 to 20 vol% PSZ in the low-frequency region.

Oxygen diffusivities and surface exchange coefficients in porous low-PSZ composites can be measured using the conductivity relaxation method. However, the oxygen diffusivities in porous high-PSZ composites could not be determined because of the predominant surface exchange reaction. The surface exchange coefficients in porous high-PSZ composites can be solely determined without respect to diffusivities, because the surface exchange reaction was the rate-limiting step for porous high-PSZ composites.

For porous mullite/PSZ composites, oxygen diffusivities and surface exchange coefficients in low-PSZ composites increased with PSZ content, and the surface exchange coefficients in high-PSZ composites were approximately constant. It was found that a percolation threshold of the surface exchange coefficients took place at ~40 vol% PSZ for porous mullite/PSZ composites. The oxygen diffusivities in porous low-PSZ

composites were independent of the oxygen partial pressure at 2.02 kPa ≤ P_{O_2} ≤ 20.2 kPa. This implied that oxygen diffusion in these composites was related to the migration of oxygen vacancies since the concentration of vacancies in low-PSZ composites was independent of the oxygen partial pressure. The surface exchange coefficients in porous high-PSZ composites decreased with increasing oxygen partial pressure with the slopes of the logα-logP_{O_2} plots slightly deviating from -1/4. It was inferred that the rate-limiting step for oxygen surface exchange could be the charge-transfer process.

References:

1. H. Schneider, K. Okada, and J. Pask, *Mullite and Mullite Ceramics*, John Wiley and Sons Ltd, New York, 1994.
2. H. Schneider, J. Schreuer, and B. Hildmann, "Structure and Properties of Mullite - A review," *J. Eur. Ceram. Soc.*, **28** 329-44 (2008).
3. A. Fletcher and Mitchell Market Reports (Firm), *Zirconia, 3rd ed.*, Elsevier Advanced Technology, Oxford, 1993.
4. N. Q. Minh, "Ceramic Fuel Cells," *J. Am. Ceram. Soc.*, **76** [3] 563-88 (1993).
5. N. Claussen and J. Jahn, "Mechanical Properties of Sintered, In Situ-Reacted Mullite-Zirconia Composites," *J. Am. Ceram. Soc.*, **63** [3-4] 228-29 (1980).
6. P. F. Becher, C. H. Hsueh, P. Angelini, and T. N. Tiegs, "Toughening Behavior in Whisker-Reinforced Ceramic Matrix Composites," *J. Am. Ceram. Soc.*, **71** [12] 1050-61 (1988).
7. M. I. Osendi, B. A. Bender, and D. Lewis III, "Microstructure and Mechanical Properties of Mullite-Silicon Carbide Composites," *J. Am. Ceram. Soc.*, **72** [6] 1049-54 (1989).
8. A. H. Heuer, F. F. Lange, M. V. Swain, and A. G. Evans, "Transformation Toughening: An Overview," *J. Am. Ceram. Soc.*, **69** [3] i-iv (1986).
9. R. Ruh, K. S. Mazdiyasni, and M. G. Mendiratta, "Mechanical and Microstructural Characterization of Mullite and Mullite-SiC-Whisker and ZrO_2-Toughened-Mullite-SiC-Whisker Composites," *J. Am. Ceram. Soc.*, **71** [6] 503-12 (1988).
10. C. C. Lin, A. Zangvil, and R. Ruh, "Modes of Oxidation in

SiC-Reinforced Mullite/ZrO_2 Composites: Oxidation vs Depth Behavior," *Acta Mater.*, **47** [6] 1977-86 (1999).

11. C. Y. Tsai, C. C. Lin, A. Zangvil, and A. K. Li, "Effect of Zirconia Content on the Oxidation Behavior of Silicon Carbide / Zirconia / Mullite Composites," *J. Am. Ceram. Soc.*, **81** [9] 2413-20 (1998).
12. C. Y. Tsai and C. C. Lin, "Dependence of Oxidation Modes on Zirconia Content in Silicon Carbide/Zirconia/Mullite Composites," *J. Am. Ceram. Soc.*, **81** [12] 3150-56 (1998).
13. H. Suito, R. Inoue, and A. Nagatani, "Mullite as an Electrochemical Probe for the Determination of Low Oxygen Activity in Liquid Iron," *Steel Res.*, **63** [10] 419-25 (1992).
14. Y. Hirata and M. Matsuda, "Electromotive Force Measurement of Mullite Ceramics as Oxygen Solid Electrolyte," *J. Ceram. Soc. Jpn.*, **101** [2] 233-36 (1993).
15. C. C. Lin, A. Zangvil, and R. Ruh, "Microscopic Mechanisms of Oxidation in SiC-Whisker-Reinforced Mullite/ZrO_2 Matrix Composites," *J. Am. Ceram. Soc.*, **82** [10] 2833-40 (1999).
16. C. C. Lin, A. Zangvil, and R. Ruh, "Phase Evolution in Silicon Carbide-Whisker-Reinforced Mullite/Zirconia Composite during Long-Term Oxidation at 1000^{o}C to 1350^{o}C," *J. Am. Ceram. Soc.*, **83** [7] 1797-803 (2000).
17. P. Mogilevsky and A. Zangvil, "Modeling of Oxidation Behavior of SiC-Reinforced Ceramic Matrix Composites," *Mater. Sci. Eng. A*, **262** 16-24 (1999).
18. P. Fielitz, G. Borchardt, M. Schmucker, H. Schneider, M. Wiedenbeck, D. Rhede, S. Weber, and S. Scherrer, "Secondary Ion Mass Spectroscopy Study of Oxygen-18 Tracer Diffusion in 2/1-mullite

Single Crystals," *J. Am. Ceram. Soc.*, **84** [12] 2845-48 (2001).

19. Y. Ikuma, E. Shimada, S. Sakano, M. Oishi, M. Yokoyama, and Z. Nakagawa, "Oxygen Self-diffusion in Cylindrical Single-Crystal Mullite," *J. Electrochem. Soc.*, **146** [12] 4672-75 (1999).
20. B. K. Kim, S. J. Park, and H. Hamaguchi, "Raman Spectrometric Determination of the Oxygen Self-Diffusion Coefficients in Oxide," *J. Am. Ceram. Soc.*, **77** [10] 2648-52 (1994).
21. J. Crank, *The Mathematics of Diffusion*, Oxford University Press, New York, 1975.
22. P. Fielitz, G. Borchardt, M. Schmucker, and H. Schneider, "How to Measure Volume Diffusivities and Grain Boundary Diffusivities of Oxygen in Polycrystalline Oxides," *Solid State Ion.*, **160** 75-83 (2003).
23. S. Kirkpatrick, "Percolation and Conduction," *Rev. Mod. Phys.*, **45** [4] 574-88 (1973).
24. V. K. S. Shante and S. Kirkpatrick, "An introduction to percolation theory," *Adv. Phys.*, **20** [85] 325-57 (1971).
25. R. Landauer, "Electrical Conductivity in Inhomogeneous Media"; pp. 2-45 in *American Institute of Physics Conference Proceedings, No. 40, Electrical Transport and Optical Properties of Inhomogeneous Media*. Edited by J. C. Garland and D. B. Tanner. American Institute of Physics, New York, 1978.
26. R. P. Kusy, "Influence of Particle Size Ratio on the Continuity of Aggregates," *J. Appl. Phys.*, **48** [12] 5301-05 (1977).
27. F. Carmona, R. Canet, and P. Delhaes, "Piezoresistivity of Heterogeneous Solids," *J. Appl. Phys.*, **61** [7] 2550-57 (1987).
28. E. L. Williams, "Diffusion of Oxygen in Fused Silica," *J. Am. Ceram. Soc.*, **48** [4] 190-94 (1965).

29. P. Fielitz and G. Borchardt, "On the Accurate Measurement of Oxygen Self-Diffusivities and Surface Exchange Coefficients in Oxides via SIMS Depth Profiling," *Solid State Ion.*, **144** 71-80 (2001).
30. M. Ishitsuka, T. Sato, T. Endo, and M. Shimada, "Sintering and Mechanical Properties of Yttria-Doped Tetragonal $Zr0_2$ Polycrystal/Mullite Composites," *J. Am. Ceram. Soc.*, **70** [11] C342-C46 (1987).
31. N. Kapuri, K. N. Rai, and G. S. Upadhyaya, "Sintering of Mullite-Based Particulate Composites Containing ZrO_2," *J. Mater. Sci.*, **31** 1481-87 (1996).
32. M. Hamidouche, N. Bouaouadja, H. Osmani, R. Torrecillias, and G. Fantozzi, "Thermomechanical Behaviour of Mullite-Zirconia Composite," *J. European Ceram. Soc.*, **16** 441-45 (1996).
33. A. Leriche, "Mechanical Properties and Microstructures of Mullite-Zirconia Composites"; pp. 541-52 in *Ceramic Transactions, Vol. 6, Mullite and Mullite Matrix Composites*. Edited by S. Somiya, R. F. Davis, and J. A. Pask. The American Ceramic Society, Westerville, 1990.
34. V. E. J. Chiochetti and E.C. Henry, "Electrical Conductivity of Some Commercial Refractories in the Temperature Range 600° to 1500°C," *J. Am. Ceram. Soc.*, **36** [6] 180-84 (1953).
35. S. P. Chaudhuri, S. Banfyopadhyay, and N. Mitra, "Electrical Resistivity of Mullite Obtained by Sintering Al_2O_3-SiO_2 Mixtures," *Interceram.*, **44** [5] 300-06 (1995).
36. R. A. Gerhardt and R. Ruh, "Volume Fraction and Whisker Orientation Dependence of the Electrical Properties of SiC-Whisker-Reinforced Mullite Composites," *J. Am. Ceram. Soc.*, **84** [10] 2328-34 (2001).

37. R. R. Turnmala, "Ceramic and Glass-Ceramic Packaging in the 1990s," *J. Am. Ceram. Soc.*, **74** [5] 895-908 (1991).
38. H. Matsumoto, Y. Iino, C. Fujiwara, Z. Kabeya, and T. Onda, "Experience on the High-Power SiC Microwave Dummy-Load Using SiC Absorber"; pp. 842-44 in *Proceedings of the 1999 Particle Accelerator Conference*. Edited by A. Luccio and W. MacKay. IEEE, Piscataway, NJ, 1999.
39. S. P. Chaudhuri, S. K. Patra, and A. K. Chakraborty, "Electrical Resistivity of Transition Metal Ion Doped Mullite," *J. Eur. Ceram. Soc.*, **19** 2941-50 (1999).
40. R. Gerhardt, "Microstructeural Characterization of Composites via Electrical Measurements," *Ceram. Eng. Sci. Proc.*, **15** [5] 1174-81 (1994).
41. J. Runyan, R. A. Gerhardt, and R. Ruh, "Electrical Properties of Boron Nitride Matrix Composites: I, Analysis of McLachlan Equation and Modeling of the Conductivity of Boron Nitride-Boron Carbide and Boron Nitride-Silicon Carbide Composites," *J. Am. Ceram. Soc.*, **84** [7] 1490-96 (2001).
42. ZView, Version 2.1b, Scribner Associates, Inc.
43. E. P. Butler and N. Bonanos, "The Characterization of ZrO_2 Engineering Ceramics by A.C. Impedance Spectroscopy," *Mater. Sci. Eng.*, **71** 49-56 (1985).
44. X. Guo and Z. Zhang, "Grain Size Dependent Grain Boundary Defect Structure: Case of Doped Zirconia," *Acta Mater.*, **51** 2539-47 (2003).
45. M. I. Osendi and J. R. Jurado, "AC Impedance Complex Plane Studies on Alumina-Zirconia and Mullite-Zirconia Composites"; pp. 239-48 in *Zirconia '88: Advances in Zirconia Science and Technology*. Edited by

S. Meriani and C. Palmonari. Elsevier Applied Science, London, 1989.

46. M. J. Ribeiro, J. C. C. Abrantes, J. M. Ferreira, and J. A. Labrincha, "Predicting Processing-Sintering-Related Properties of Mullite-Alumina Ceramic Bodies Based on Al-Rich Anodising Sludge by Impedance Spectroscopy," *J. Eur. Ceram. Soc.*, **24** [15-16] 3841-48 (2004).
47. G. Y. Meng and R. A. Huggins, "The Oxygen Ion Conductivity of Mullite Prepared Using a Wet Chemical Process," *Solid State Ion.*, **11** 271-78 (1984).
48. Y. Hirata, M. Kawabata, and Y. Ishihara, "Electrical Properties of Silica-Alumina Ceramics in Nitrogen Atmosphere," *J. Mater. Res.*, **8** [5] 1116-21 (1993).
49. J. R. Macdonald, *Impedance Spectroscopy: Emphasizing Solid Materials and Systems*, John Wiley & Sons, New York, 1987.
50. S. Prochazka, J. S. Wallace, and N. Claussen, "Microstructure of Sintered Mullite-Zirconia Composites," *J. Am. Ceram. Soc.*, **66** [8] C125-C27 (1983).
51. A. Zangvil, C. C. Lin, and Robert Ruh, "Microstructural Studies in Alkoxide-Derived Mullite/Zirconia/Silicon Carbide-Whisker Composites," *J. Am. Ceram. Soc.*, **75** [5] 1254-63 (1992).
52. D. S. McLachlan, M. Blaszkiewicz, and R. E. Newnham, "Electrical Resistivity of Composites," *J. Am. Ceram. Soc.*, **73** [8] 2187-203 (1990).
53. K. Lichtenecker, "Dielectric Constant of Natural and Synthetic Mixtures," *Phys. Z.*, **27** 115-58 (1926).
54. K. S. Moon, H. D. Choi, A. K. Lee, K. Y. Cho, H. G. Yoon, and K. S. Suh, "Dielectric Properties of Epoxy-Dielectrics-Carbon Black Composite for Phantom Materials at Radio Frequencies," *J. Appl.*

Polym. Sci. , **77** 1294-302 (2000).

55. H. Kobayashi and Y. Hosokawa, "Dielectric Constant Characteristics of a New Composite Dielectric Material," *J. Am. Ceram. Soc.*, **73** [6] 1774-76 (1990).
56. T. Zakri, J. P. Laurent, and M. Vauclin, "Theoretical Evidence for 'Lichtenecker's Mixture Formulae' Based on the Effective Medium Theory," *J. Phys. D: Appl. Phys.*, **31** 1589-94 (1998).
57. H. D. Ko and C. C. Lin, "Oxygen Diffusivities in Mullite/Zirconia Composites Measured by $^{18}O/^{16}O$ Isotope Exchange and Secondary Ion Mass Spectrometry," *J. Mater. Res.*, **23** [2] 353-58 (2008).
58. I. A. Aksay, D. M. Dabbs, and M. Sarikaya, "Mullite for Structural, Electronic, and Optical Applications," *J. Am. Ceram. Soc.*, **74** [10] 2343-58 (1991).
59. Q. M. Yuan, J. Q. Tan, and Z. G. Jin, "Preparation and Properties of Zirconia-Toughened Mullite Ceramics," *J. Am. Ceram. Soc.*, **69** [3] 265-67 (1986).
60. M. Ishitsuka, T. Sato, T. Endo, and M. Shimada, "Sintering and Mechanical Properties of Yttria-Doped Tetragonal ZrO_2 Polycrystal/Mullite Composites," *J. Am. Ceram. Soc.*, **70** [11] C342-C46 (1987).
61. H. D. Ko, C. C. Lin, and K. C. Chiu, "Effect of Zirconia Content on Electrical Conductivities of Mullite/Zirconia Composites Measured by Impedance Spectroscopy," *J. Mater. Res.*, **23** [8] 2125-32 (2008).
62. J. J. Haslam and F. F. Lange, "Strengthening of Porous Mullite and Zirconia CMC Matrices by Evaporation/Condensation," *J. Am. Ceram. Soc.*, **89** [6] 2043-50 (2006).
63. B. A. Latella and E. G. Mehrtens, "High Temperature Biaxial Strength

of Porous Mullite-Alumina and Mullite-Zirconia Ceramics," *J. Mater. Sci.*, **42** 5880-82 (2007).

64. R. Ganeshananthan and A. V. Virkar, "Measurement of Surface Exchange Coefficient on Porous $La_{0.6}Sr_{0.4}CoO_{3-\delta}$ Samples by Conductivity Relaxation," *J. Electrochem. Soc.*, **152** [8] A1620-A28 (2005).
65. S. Wang, A. Verma, Y. L. Yang, A. J. Jacobson, and B. Abeles, "The Effect of the Magnitude of the Oxygen Partial Pressure Change in Electrical Conductivity Relaxation Measurements: Oxygen Transport Kinetics in $La_{0.5}Sr_{0.5}CoO_{3-\delta}$," *Solid State Ion.*, **140** [1-2] 125-33 (2001).
66. J. Crank, *The Mathematics of Diffusion*, 60. Oxford University Press, New York, 1975.
67. B. C. H. Steele, "Interfacial Reactions Associated with Ceramic Ion Transport Membranes," *Solid State Ion.* , **75** 157-65 (1995).
68. H. J. M. Bouwmeester and A. J. Burggraaf, "Dense ceramic membranes for oxygen separation"; pp. 481 in *The CRC Handbook of Solid State Electrochemistry*. Edited by P. J. Gellings and H. J. M. Bouwmeester. CRC Press, Boca Raton, Florida, 1997.
69. M. W. den Otter, H. J. M. Bouwmeester, B. A. Boukamp, and H. Verweij, "Reactor Flush Time Correction in Relaxation Experiments," *J. Electrochem. Soc.*, **148** [2] J1-J6 (2001).
70. A. Kopp, H. Nafe, and W. Weppner, "Characterization of the electronic charge carriers in TZP," *Solid State Ion.*, **53-56** 853-58 (1992).
71. C. Schwandt and W. Weppner, "Electrode Reactions at Oxygen, Noble Metal / Stabilized Zirconia Interfaces," *Ionics*, **2** 113-22 (1996).
72. A. S. Patnaik and A. V. Virkar, "Transport Properties of Potassium-Doped $BaZrO_3$ in Oxygen- and Water-Vapor-Containing

Atmospheres," *J. Electrochem. Soc.*, **153** [7] A1397-A405 (2006).

73. H. E. Exner, "Stereology and 3D Microscopy: Useful Alternatives or Competitors in the Quantitative Analysis of Microstructures?," *Image Anal. Stereol.*, **23** 73-82 (2004).
74. H. Schmalzried, *Monographs in Modern Chemistry; Vol. 12 : Solid State Reactions*, 59. Verlag Chemie, Weinheim, 1981.
75. T. Horita, K. Yamaji, N. Sakai, M. Ishikawa, H. Yokokawa, T. Kawada, and M. Dokiya, "Oxygen Surface Exchange of $Y_{0.2}Ce_{0.8}O_{2-x}$ under Reducing Atmosphere," *Electrochem. Solid State Lett.* , **1** [1] 4-6 (1998).
76. A. Karthikeyan and S. Ramanathan, "Oxygen surface exchange studies in thin film Gd-doped ceria," *Appl. Phys. Lett.*, **92** 243109 (2008).
77. J. D. Sirman and J. A. Kilner, "Surface Exchange Properties of $Ce_{0.9}Gd_{0.1}O_{2-x}$ Coated with $La_{1-x}Sr_xFe_yCo_{1-y}O_{3-\delta}$," *J. Electrochem. Soc.*, **143** [10] L229-L31 (1996).
78. O. J. Velle, T. Norby, and P. Kofstad, "The Electrode System O_2/Pt//ZrO_2:8Y_2O_3 Investigated by Impedance Spectroscopy," *Solid State Ion.*, **47** 161-67 (1991).
79. S. P. Yoon, S. W. Nam, S. G. Kim, S. A. Hong, and S. H. Hyun, "Characteristics of Cathodic Polarization at Pt/YSZ Interface without the Effect of Electrode Microstructure," *J. Power Sources*, **115** 27-34 (2003).
80. E. L. Cussler, *Diffusion: Mass Transfer in Fluid Systems; 2nd Ed.*, 101. Cambridge University Press, Cambridge, U.K., 1997.
81. J. Mizusaki, K. Amano, S. Yamauchi, and K. Fueki, "Electrode Reaction at Pt, $O_{2(g)}$/Stabilized Zirconia Interfaces. Part I: Theoretical Consideration of Reaction Model," *Solid State Ion.*, **22** 313-22 (1987).

82. J. Mizusaki, K. Amano, S. Yamauchi, and K. Fueki, "Electrode Reaction at Pt, O2(g)/Stabilized Zirconia Interfaces. Part II: Electrochemical Measurements and Analysis," *Solid State Ion.*, **22** 323-30 (1987).

List of Publications

1. H. D. Ko and C. C. Lin, "Oxygen Diffusivities in Mullite/Zirconia Composites Measured by $^{18}O/^{16}O$ Isotope Exchange and Secondary Ion Mass Spectrometry," *J. Mater. Res.*, **23** [2] 353-58 (2008).

2. H. D. Ko, C. C. Lin, and K. C. Chiu, "Effect of Zirconia Content on Electrical Conductivities of Mullite/Zirconia Composites Measured by Impedance Spectroscopy," *J. Mater. Res.*, **23** [8] 2125-32 (2008).

3. H. D. Ko and C. C. Lin, "Oxygen Diffusivities and Surface Exchange Coefficients in Porous Mullite/Zirconia Composites Measured by the Conductivity Relaxation Method." Accepted by *J. Am. Ceram. Soc.* (2009).